Title: **Activation and regulation of a p38α MAPK by its downstream MAPKAP kinase through feedback phosphorylation and LLPS-driven condensate formation.**

Pranita Ray[a], Pallavi Rao T[b,c], Mintu Nandi[d], Afreen Haque[a], Samrat Mitra[a], Swasti Raychaudhuri[b,c], Anindya Ghosh-Roy[e] and Smarajit Polley[a,1]

a Department of Biological Sciences, Bose Institute, Sector V, Bidhan Nagar, Kolkata 700091, India; b CSIR-Centre for Cellular and Molecular Biology, Uppal Road, Hyderabad 500007, India; c Academy of Scientific and Innovative Research (AcSIR), Ghaziabad- 201002, India; d Department of Chemistry, Indian Institute of Engineering Science and Technology, Shibpur, Howrah 711103, India; e Department of Cellular and Molecular Neuroscience, National Brain Research Centre, Manesar 122052, India.

1 corresponding author: smarajit.polley@gmail.com, spolley@jcbose.ac.in

**Highlights:**

- PMK3 participates in a feedback phosphorylation loop with its downstream kinase MAK2 that leads to the phosphorylation of the activating TxY motif.
- MAK2 Phosphorylates PMK-3 at Ser, Thr and Tyr residues and that is a dual specificity kinase rather than a Ser/Thr kinase.
- MAK2 but not PMK3 alone forms condensates through liquid liquid phase separation (LLPS).
- While PMK3 alone is prone to aggregation, MAK2 prevents aggregation of PMK3 via LLPS-mediated condensate formation when present together.

**Abstract:**

**MAP kinases (MAPKs) represent a class of evolutionarily conserved signaling molecules that respond to an array of extracellular stimuli and stresses. p38 group of MAPKs have been implicated in a multitude of signal transduction pathways known to be activated by dual-specific upstream MAPK kinases and also by autophosphorylation. They activate MAPK activated protein kinases (MAPKAPKs) in a context dependent manner by specific phosphorylation, and together they play crucial**

**biological roles. One such pair in *C. elegans* consists of PMK3, p38α-MAPK and its cognate MAPKAPK, MAK2 downstream of DLK1 (MAPK kinase kinase) and MKK4 (MAPK kinase). They are implicated in axonal regeneration, degeneration and synaptic pruning in response to neuronal injury. Here, we report that PMK3 participates in a feedback loop with MAK2 leading to phosphorylation-mediated activation of both kinases. Interestingly, MAK2 that is a Ser/Thr kinase phosphorylates PMK3 at its TxY-motif required for the manifestation of full activity of PMK3. This observation identifies MAK2 as a dual specificity kinase. Distribution of phosphorylation sites on either kinase and presence of long intrinsically disordered regions in each of them indicate the possibility of conformational plasticity in the PMK3:MAK2 complex. Furthermore, MAK2 increases bioavailability of aggregation-prone PMK3 by forming LLPS-driven condensates. PMK3 and MAK2 retain the feedback phosphorylation relationship and enzymatic activities in the condensate state as well. Our observations establish an unreported feedback relationship between a MAPK and its downstream MAPKAPK through phosphorylation and LLPS-driven condensate formation.**

**Significance Statement:**

**MAPK family of protein kinases are evolutionarily conserved and participate in a diverse array of signaling events. p38 MAPKs are key players in cellular phenomenon involving cell survival, differentiation, metabolic processes, and neuronal response to injury. They are activated through phosphorylation by upstream MAPK kinases (MAP2Ks) or by autophosphorylation. We found that a *C. elegans* MAPK (PMK3) engages in a feedback phosphorylation loop with its downstream effector kinase MAK2, but not the upstream MAP2K MKK4, that ensures robust activation of PMK3 by MAK2 without requiring MKK4. In addition, MAK2 increases bioavailability of activation-competent and active PMK3 by preventing its aggregation through LLPS-driven condensate formation. This feedback relationship between a MAPK and its downstream MAPKAPK might ensure rapid activation of this pathway in response to nervous system injury or stress.**

**Introduction:**

Protein kinases are implicated in almost, if not all, signaling events in eukaryotes (Manning et al., 2002). Mitogen activated protein kinases (MAPKs) are activated by a variety of extracellular stimuli that regulate a plethora of cellular processes including but not limited to gene expression, cell cycle, cell survival, infection, inflammation, apoptosis, differentiation and metabolism (Battagello et al., 2020; Bouhaddou et al., 2020; Cuadrado and Nebreda, 2010; Luecke et al., 2024; Widmann et al., 1999). They are one of the most ancient signal transduction molecules observed throughout evolution. Multiple MAPK pathways are found to operate in concert in eukaryotes. A canonical MAPK module consists of two upstream kinases, MAPK kinase (MAPKK or MAP2K) and MAKK kinase (MAPKKK or MAP3K)(Pearson et al., 2001). In response to extracellular stimuli, a MAP3K activates its cognate MAP2K that in turn activates the downstream MAPK – making it a three-kinase signaling module where the signal transmits from the MAP3K to MAPK via the MAP2K. Activation of p38$\alpha$ by autophosphorylation has also been documented (Ge et al., 2002) apart from the canonical mode of MAPK activation by MAP2K suggesting multiple modes of MAPK-activation in play. MAPKs are Ser/Thr kinases that phosphorylate different kinds of protein substrates in cells including transcription factors and specific protein kinases called the MAPK activated protein kinases (MAPKAPKs) (Cargnello and Roux, 2011).

p38 group of MAPKs are perhaps the most widely implicated and most well-studied pathways among the four distinct subgroups of the MAPK family (Canovas and Nebreda, 2021; Cuadrado and Nebreda, 2010). In mammals, there are four isoforms of p38: $\alpha$, $\beta$, $\gamma$ and $\delta$. Among these p38$\alpha$ is the most well studied one. Among many substrates of p38$\alpha$ MAPKAPK2 or MK2 have been implicated in many cellular processes that phosphorylate substrates including small heat shock protein 27 (Hsp27), cAMP response element-binding protein (CREB), lymphocyte-specific protein 1 (LSP1), transcription factor ATF1 etc (Zarubin and Han, 2005). p38 MAPKs are present both in the cytoplasm and nuclei of cells and are sequestered mostly in the nuclei in certain stress conditions. Nucleocytoplasmic shuttling of the p38 MAPKs is also regulated by their association with the MAPKAPKs (Ben-Levy et al., 1998).

*C. elegans* genome consists of three genes, *pmk1, pmk2* and *pmk3* that code for three p38 MAPK isoforms: PMK1, PMK2 and PMK3, respectively. These three genes constitute an operon with a polarity from *pmk1* to *pmk3*, and are expressed under the influence of a single promoter (Berman et al., 2001). Among these three p38 MAPK isoforms PMK3 has been implicated in axonal regeneration acting as the MAPK downstream of MAP2K, MKK4 that is activated by the MAP3K, DLK1 in both *C. elegans* and other organisms (Hammarlund et al., 2009; Hao et al., 2016; Shin et al., 2012; Yan et al., 2009). This signaling mechanism is also

implicated in synaptic maturation in multiple organisms, which is under the tight regulation of E3 ubiquitin ligase (Lewcock et al., 2007; Nakata et al., 2005; Schaefer et al., 2000). In the axonal regeneration pathway involving DLK-1, the terminal kinase however is not the MAPK but a cognate MAPKAPK of PMK3 known as MAK2 (Fig 1A). MAK2 is involved in the maintenance of the neuronal synapses and axon morphology. It has also been shown that MAK2 regulates touch neuron axon regeneration by modulating *cebp-1* mRNA stability in response to axon injury in nematode (Yan et al., 2009). A search for the protein-protein interaction networks related to PMK3 and MAK2 on the STRING database revealed strong interactions between the two proteins (Fig S1A). We asked the question, whether activation, regulation and mutual relationship of p38$\alpha$ and its MAPKAPK established in mammalian systems also holds true in the PMK3:MAK2 system, which is involved in multiple cellular responses such as axon regeneration (Hammarlund et al., 2009), degeneration (Asghari Adib et al., 2018), and synaptic pruning (Asghari Adib et al., 2024) following neuronal injury. We used the nematode specific counterparts of MAPK and MAPKAP as our model system. Our biochemical, computational and mass spectrometric analyses revealed that PMK3 participates in a hitherto unknown feedback phosphorylation loop with its downstream kinase MAK2 that leads to the phosphorylation of the activating TxY motif. This observation in turn proved that MAK2 is a dual specificity kinase rather than a Ser/Thr kinase as it is annotated in the different databases. We also found that, MAK2 but not PMK3 forms condensates through liquid liquid phase separation (LLPS). Intriguingly, while PMK3 alone is prone to aggregation -- MAK2 prevents aggregation of PMK3 via LLPS-mediated condensate formation when present together. The feedback phosphorylation relationship remains functional in the condensate state. These observations point towards an unknown regulatory aspect of a kinase (PMK3) wherein it is regulated by its cognate downstream kinase (MAK2) not only by means of its catalytic activity to chemically modify (activating phosphorylation) but also through change of physico-chemical microenvironment in the form of condensates. Overall, our study revealed a new mechanistic understanding of the regulation of the injury sensing MAPK PMK-3 via its downstream kinase MAPKAP MAK-2.

## Results:

### *In vitro* reconstitution of a MAPK-MAPKAPK module implicated in axonal regeneration in *C. elegans*:

PMK3 (Uniprot id: O44514, M.W. 54.9kDa) is a p38 MAPK in *C. elegans* (Fig 1B). It participates in the DLK1-dependent signaling cascade in axonal regeneration pathway downstream of the MAP2K, MKK4 (KEGG pathway cel04361) (Hammarlund et al., 2009; Yan et al., 2009). DLK1 acts as the MAP3K in the said pathway. PMK3 phosphorylates a downstream kinase MAK2 (Uniprot id: Q965G5, M.W. 41.5kDa), a MAP kinase activated

protein kinase (MAPKAPK) (Fig 1B). The involvement of MAK2 in this cascade turns the canonical three-kinase MAPK-module into a four-kinase module. To understand the mutual relationship between these two terminal kinases in further details, we sought to purify PMK3 and MAK2 recombinantly (see materials and methods). Of note, PMK3 showed highest similarity with the p38α MAPK when compared with the four p38 MAPKs of the human origin (Fig S1B). PMK3 was overexpressed in *E. coli* and purified as a 6X-His tagged protein from the soluble fraction. Interestingly, fractions eluted from Ni-NTA column (Fig S1C, left panel)

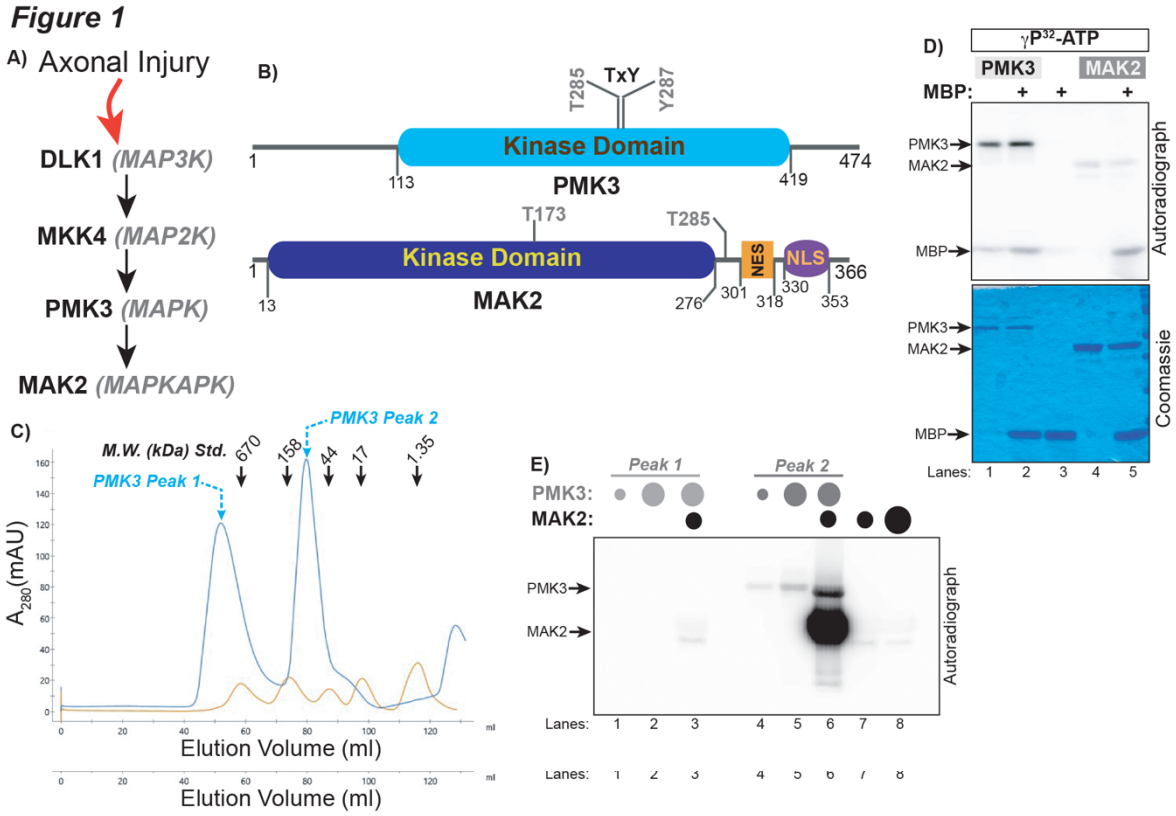


**Figure 1*: In vitro* reconstruction of a MAPK-MAPKAPK module involved in axonal regeneration in *C. elegans.***

**(A)** Schematic representation of the unique four-kinase DLK-1 MAPK signaling pathway in *C. elegans*. PMK3 (MAPK) and MAK2 (MAPKAPK) act as the two terminal kinases in this module. **(B)** Top: Domain architecture of PMK3 depicting the kinase domain and the T-X-Y motif within the activation loop. Lower panel: Domain architecture of MAK2 depicting the kinase domain, the nuclear export signal (NES) and the nuclear localization signal (NLS). The domain borders have been numbered. **(C)** Comparison of the size exclusion profiles of 6X His-PMK3 and a molecular weight standard resolved on a preparative gel filtration column. The absorbance at 280nm has been plotted against the elution volume. The larger molecular weight fractions constitute Peak 1 and the lower molecular weight fractions constitute Peak2. **(D)** *In vitro* radioactive kinase assay with purified, recombinant PMK3 and MAK2 using myelin basic protein (MBP) as a generic substrate. **(E)** *In vitro* radioactive kinase assay with purified, recombinant PMK3 and MAK2. PMK3 from two peaks in SEC was used for the assay in different reactions.

158 separated into two distinct peaks corresponding to molecular weight (MW) greater than
159 670kDa (oligomer) and greater than 44kDa but less then 158kDa (possibly a dimer) when

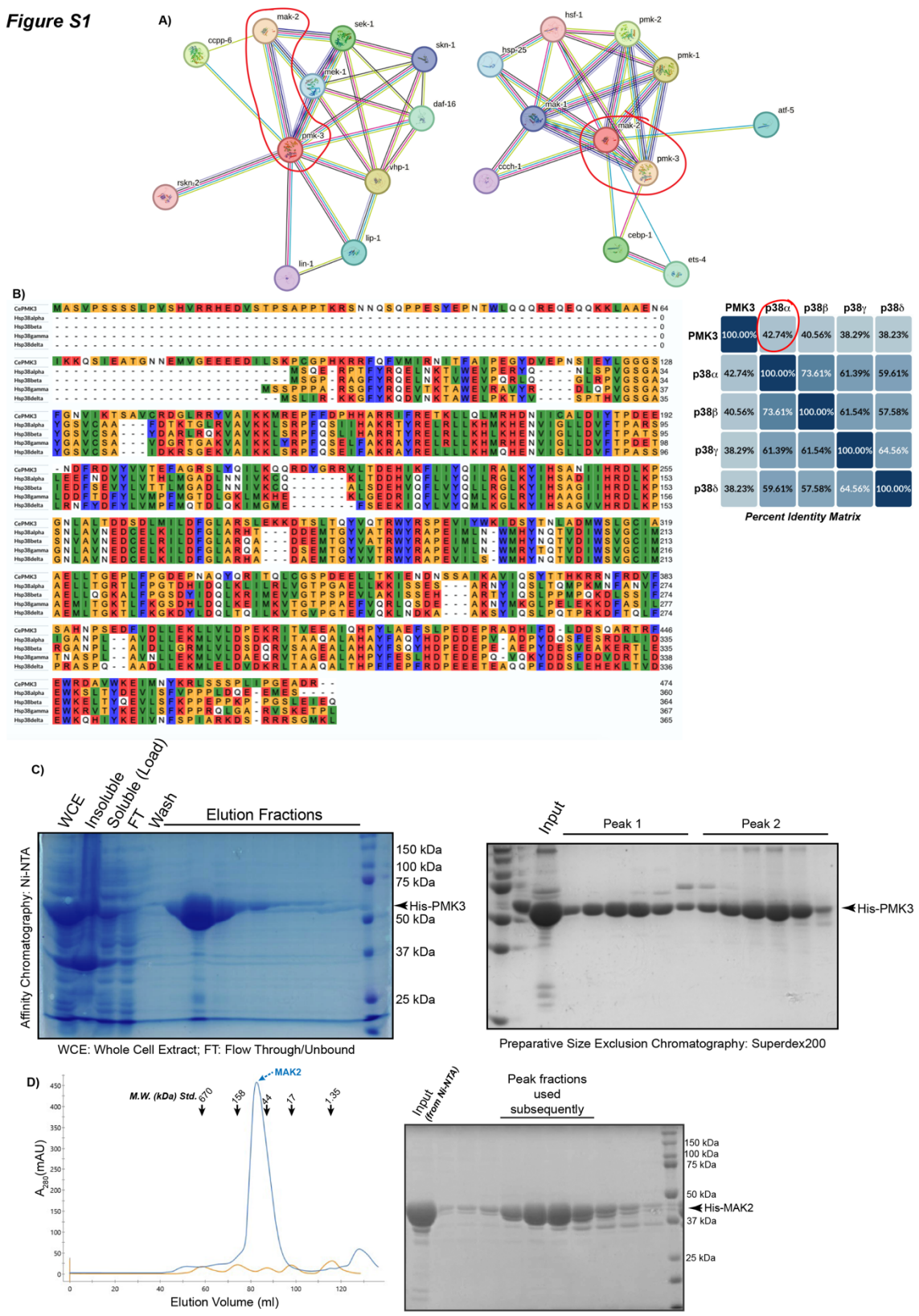


160
161 resolved on a preparative Superdex 200 SEC column (Fig 1C; corresponding Coomassie
162 brilliant blue stained SDS-PAGE is shown in Fig S1C, right panel). MAK2 was similarly purified

**Figure S1: (A)** Analysis of the protein-protein interaction network between PMK3 and MAK2 using the STRING database. **(B)** Multiple sequence alignment of C. elegans PMK3 (CePMK3) with the four human p38 (Hsp38) MAPK isoforms α, β, γ and δ (left panel). The percent identity matrix obtained from the MSA of the p38 MAPK sequences (right panel). Darker shade in the box implies higher sequence identity. PMK3 shares highest sequence similarity with human p38α. **(C)** Left panel: Coomassie brilliant blue stained SDS-PAGE of the recombinant 6X His-PMK3, purified by Ni-NTA affinity chromatography. Right panel: Coomassie stained SDS-PAGE of the size exclusion chromatography (SEC) (Run profile shown in Fig 1C). **(D)** Left panel: Comparison of the size exclusion profiles of 6X His-MAK2 and a molecular weight standard resolved on a preparative Superdex 200 column. Right panel: Coomassie brilliant blue stained SDS-PAGE showing the purified MAK2 protein fractions, following SEC.

from *E. coli*. Unlike PMK3, MAK2 eluted as a single peak when resolved on the same SEC column (Fig S1D, left panel; corresponding Coomassie brilliant blue stained SDS-PAGE is shown in Fig S1D, right panel). MAK2 and low MW fraction of PMK3 were then subjected to *in vitro* radioactive kinase assay using myelin basic protein (MBP) as a generic substrate (Cicirelli et al., 1988). Both of these kinases phosphorylated MBP, wherein PMK3 was found to phosphorylate MBP more efficiently than MAK2 (Fig 1D).

It is expected that active PMK3 would phosphorylate its downstream kinase MAK2. We wanted to confirm this phenomenon with our purified recombinant kinases. PMK3 from the two peaks eluting from the SEC column were subjected to *in vitro* kinase assays using γ-$^{32}$P-ATP as the phosphate donor and MAK2 as the substrate. Substrate phosphorylation and autophosphorylation was monitored by autoradiography (Fig 1E). PMK3 from the smaller MW peak displayed huge activity towards MAK2 (lane 6) while the same protein in the large MW fraction did not show any detectable activity in the same assay (lane 3). These observations hinted that oligomerization of PMK3 into a large self-assembly was detrimental to its activity. Interestingly, when PMK3 was subjected to same assay without the MAK2 it displayed much lower level of autophosphorylation (lanes 4,5) compared to that in the presence of MAK2 (lane 6). Furthermore, MAK2 alone showed very low level, if any, of autophosphorylation signal (lanes 7,8) in absence of PMK3. Enhancement of phosphorylation of MAK2 in presence of PMK3 was expected owing to the fact that MAK2 is an MAPK activated protein kinase and is assigned down stream of its cognate MAPK, PMK3. However, it came as a surprise when phosphorylation of PMK3 was profoundly increased in presence of its downstream substrate kinase, i.e., MAK2 pointing to a plausible feedback phosphorylation loop (Fig 1E).

**PMK3 participates in a feedback phosphorylation loop with downstream kinase MAK2 but not with upstream kinase MKK4:**

The above set of experiments hinted to the possibility of existence of a feedback phosphorylation loop between the MAPK (PMK3) and its downstream kinase MAK2. We wanted to further analyze this possibility using our *in vitro* assay system using purified

200 recombinant proteins. 1uM of PMK3 was incubated with 6uM of MAK2 in presence of $\gamma$-$^{32}$P-
201 ATP as the phosphate donor for different time intervals at 25°C, and the resulting reaction
202 mixtures were resolved on an SDS-PAGE prior to detecting the phosphorylation signal by
203 phosphor-imaging after drying the gel. Respective kinases were incubated alone at the same
204 concentration as in the mixtures for the same time intervals to assess self-phosphorylation. It
205 was observed that, both PMK3 and MAK2 were heavily phosphorylated in a time dependent
206 manner when incubated together (lanes 5-8) (Fig 2A). Those kinases, however, did not show
207 appreciable autophosphorylation when incubated alone in the same assay conditions (lanes
208 1-4 and 9-12) (Fig 2A). This result confirmed the presence of a feedback phosphorylation loop
209 between these two kinases (Fig 2A). We next wanted to check if this feedback phosphorylation
210 is dependent upon the relative stoichiometry of the two participating kinases. To this end, we
211 used equimolar concentration of the kinases (~2uM each) and followed their phosphorylation
212 in the same conditions as mentioned above. Like the last assay, both PMK3 and MAK2 were
213 heavily phosphorylated when incubated together as expected suggesting that the feedback
214 phosphorylation was independent of the relative stoichiometry of the two kinases (lanes 9-12)
215 (Fig 2B). MAK2 did not show appreciable autophosphorylation (lanes 5-8), however, PMK3
216 showed higher levels of autophosphorylation (lanes 1-4) (Fig 2B) compared to that in Fig 2A
217 raising the possibility that autophosphorylation of PMK3 could be a concentration dependent
218 phenomenon as we used more kinase in this assay (Fig 2B) that the earlier assay shown in
219 Fig 2A.
220 It was reported earlier that, active MKK4 is able to activate PMK3 by phosphorylation
221 (Nakata et al., 2005) reminiscent of similar findings in human where MKK6 phosphorylates
222 p38$\alpha$ (Han et al., 1996; Moriguchi et al., 1996a; Moriguchi et al., 1996b). We wanted to find
223 out if the newly discovered feedback loop is specific for PMK3 with its downstream kinase
224 MAK2, or it could also participate in a similar feedback loop with its upstream MAP2K MKK4
225 as well. Similar assay as above was performed using recombinantly purified PMK3 and MKK4.
226 Phosphorylation level of PMK3 was much higher in presence of MKK4 (Fig 2C, lanes 4-6)
227 compared to PMK3 alone (Fig 2C, lanes 7-9). Interestingly, while MKK4 could efficiently trans-
228 phosphorylate its downstream kinase PMK3 as expected (Fig 2C, lanes 4-6), no feedback
229 phosphorylation from PMK3 to MKK4 could be discerned in this assay as MKK4 also showed
230 comparable high signal for autophosphorylation in the absence of PMK3 (Fig 2C, lanes 1-3;
231 compare lanes 1-3 and 4-6).
232 The above set of results brings out an unreported feedback phosphorylation loop
233 between a p38 MAPK and its cognate MAPKAPK (Fig 2D). PMK3 specifically engages in such
234 a feedback relationship with its downstream MAK2 but not with its upstream MKK4 (MAP2K)

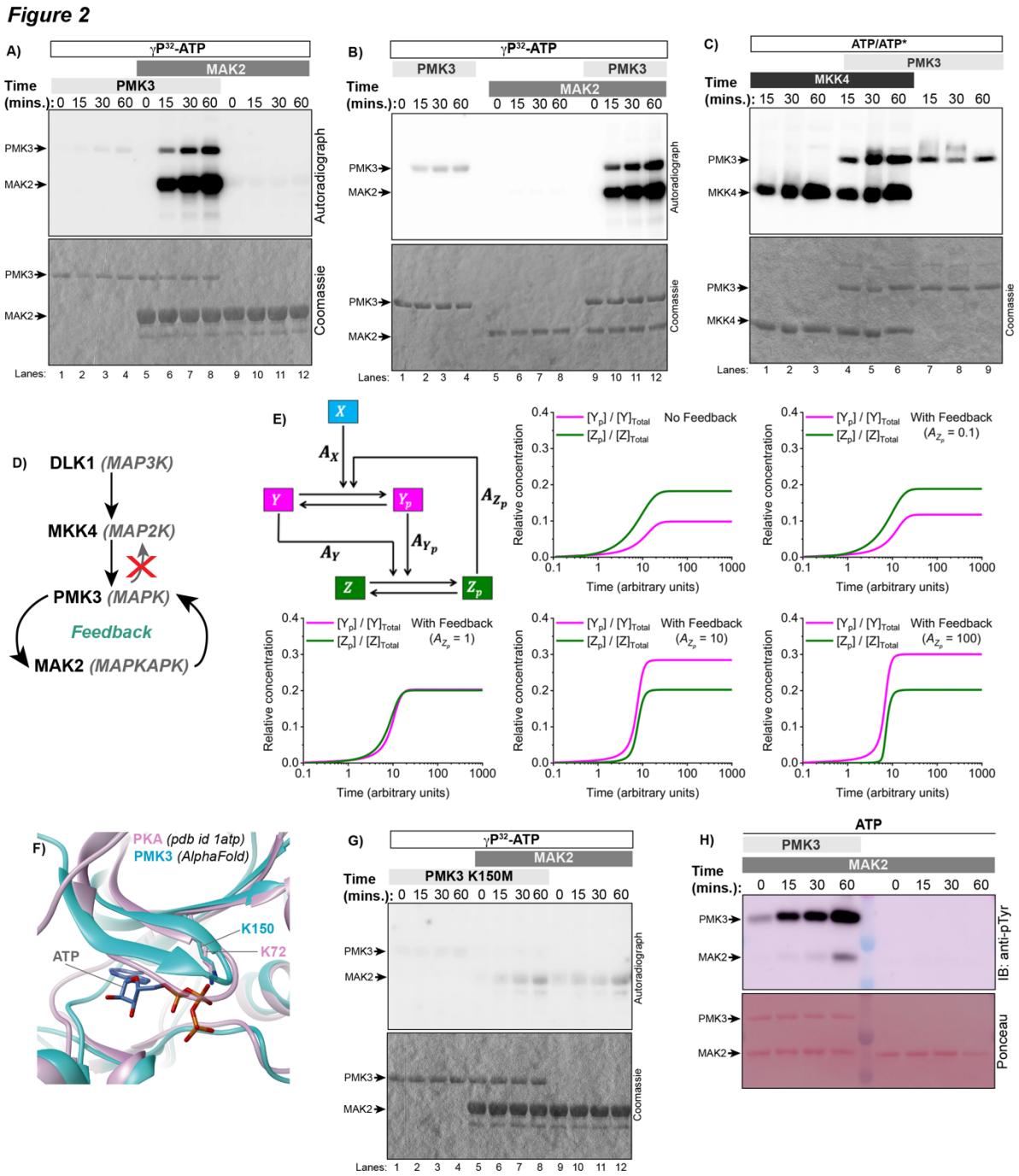


**Figure 2: PMK3 engages in feedback phosphorylation with the downstream Kinase MAK2, but not the upstream kinase MKK4.**

**(A-C)** *In vitro* radioactive phosphorylation assays with recombinant PMK3 (MAPK), MAK2 (MAPKAPK) and MKK4 (MAP2K), elaborating on the feedback loop. (A) MAK2 phosphorylates PMK3 by a feedback mechanism in a time dependent manner. (B) The feedback phosphorylation loop between PMK3 and MAK2 is independent of the relative stoichiometry of the two constituent kinases. (C) This mechanism of signal transmission is specific for PMK3 and its downstream substrate MAK2 and does not occur for the upstream kinase MKK4. **(D)** A schematic illustration depicting the phenomenon of feedback phosphorylation between PMK3 and MAK2, but not between PMK3 and MKK4. **(E)** Bioinformatic modelling of the effect of feedback loop on the overall phosphorylation kinetics of the two kinases. The temporal evolution of relative concentrations of $Y_p$ (phosphorylated PMK3) and $Z_p$ (phosphorylated MAK2) are presented with respect to total kinase amount of each kinase for different values of feedback strengths ($A_{Z_p}$), which is a dimensionless measure of feedback strength and sensitivity. **(F)** Superimposition of the AlphaFold predicted structure of *C. elegans* PMK3 on Protein kinase A (PKA) structure. The conserved ATP binding Lys residue has been marked in both the structures.

**(G)** An *in vitro* kinase assay with a kinase dead PMK3 mutant (PMK3 K150M) and MAK2 show that the presence of active PMK3 is essential for the kickstart the feedback phosphorylation loop. **(H)** MAK2 is a dual specificity kinase that phosphorylates PMK3 on tyrosine residues. PMK3 and MAK2 were incubated with non-radioactive 'cold' ATP and subjected to immunoblot analyses using anti p-tyrosine antibodies. The blot is a representative of three independent experiments.

(Fig 2D). In order to understand the effect of such feedback relationship, we modeled the system as depicted in Fig 2E; wherein X denotes MKK4 (MAP2K), Y denotes PMK3 (MAPK) and Z denotes MAK2 (MAPKAPK). $Y_p$ and $Z_p$ represent the phosphorylated versions of the respective kinases and are considered active. For simplicity, we did not differentiate between multiple phosphorylated versions, if any. We modeled the entire scheme by writing down coupled ordinary differential equations. The model clearly captures the effect of feedback on the phosphorylation kinetics and relative amounts of phosphorylated kinases (with respect to the total kinase amount) (Fig 2E). The effect of feedback is accounted by considering a dimensionless parameter $A_{Z_p}$, called feedback strength and sensitivity (for details see materials and methods). Clearly, such feedback is advantageous to generate active pools of those kinases than without feedback.

It is understood that activities of both kinases are required to propagate this feedback phosphorylation loop between PMK3 and MAK2. However, it is not clear activity of which kinase is mandatory for kickstarting this feedback loop: whether the upstream kinase (PMK3) must phosphorylate the downstream kinase (MAK2) first or *vice versa* to make this feedback loop operative. To analyze these possibilities, we took advantage of a mutant PMK3 where invariant ATP binding Lys, K150 was replaced by Met giving rise to PMK3 K150M mutant kinase. This ATP-anchoring Lys is conserved in all eukaryotic protein kinases that positions the ATP in the kinase (Fig 2F) resulting in a productive phospho-transfer reaction. Mutation of this invariant residue leads to abrogation of kinase activity, in essence such mutants are either kinase dead or retain minimal activity, if any. We performed a similar *in vitro* phosphorylation assay with PMK3 K150M and MAK2 using radioactive ATP. We observed that, the feedback phosphorylation of the respective kinases did not occur (Fig 2G, lanes 5-8). Furthermore, no autophosphorylation signal was observed for PMK3 when it was incubated with radioactive ATP in the absence of MAK2 (Fig 2G, lanes 1-4). MAK2 underwent faint autophosphorylation when incubated alone (Fig 2G, lanes 9-12), which was comparable to that in the reactions in presence of its dead upstream kinase (Fig 2G, compare lanes 5-8 and 9-12). This experiment proved that initiation and further propagation of the feedback phosphorylation loop is critically dependent upon active PMK3. We surmise that active PMK3 is necessary and active MAK2 is not sufficient to initiate this feedback phosphorylation loop though it is understandable that activities of both kinases would be required for the maintenance/propagation of the feedback loop.

280 We have established the specific feedback phosphorylation relationship between
281 PMK3 and MAK2; however, it is unclear what could be the possible role of PMK3-
282 phopshorylation by MAK2. It is known that MAPKs require TxY phosphorylation to become
283 fully active and it is canonically done by its upstream dual specificity kinase MAP2K (here
284 MKK4). On the other hand, MAK2 which is placed downstream of PMK3 is annotated as a
285 Ser/Thr kinase in the UniProt database (EC number EC:2.7.11.1). In order to activate PMK3
286 fully, MAK2 must phosphorylate PMK3 at Thr as well as Tyr. As we lacked any specific
287 antibody to detect the phosphorylated TxY motif of PMK3, we tested the pan-tyrosine
288 phosphorylation of PMK3 by MAK2. We found that, MAK2 is capable of phosphorylating PMK3
289 on tyrosine residues (Fig 2H). This unexpected discovery identifies MAK2 as a dual specificity
290 kinase rather than a Ser/Thr kinase and raises the possibility that MAK2 might be capable of
291 activating PMK3 to ensure robust activation of such an important kinase.
292
293 **Mass spectrometric analyses of PMK3 and MAK2 phosphorylation:**
294 p38-MAPKs require phosphorylation of the TxY motif in their activation loop to unleash
295 their kinase-activity. Phosphorylation of both T and Y in the motif usher maximum activity while
296 phosphorylation of only T show much reduced activity and that of only Y renders the kinase
297 inactive (Zhang et al., 2008). In the previous sections we have seen that PMK3 and MAK2
298 engage in an unreported feedback phosphorylation relationship. It was also observed that,
299 phosphorylation on both PMK3 and MAK2 increased many folds when they were both present
300 in the reaction compared to the lone-kinases. However, it is unknown which sites in these
301 kinases get phosphorylated in such a situation. To this end, we performed high resolution LC-
302 MS/MS experiments after digesting a mixture of PMK3 and MAK2 with Trypsin after the
303 mixture was incubated with ATP. Resulting phospho-peptides were enriched after Trypsin-
304 digestion using Fe-NTA column before separation on a nano-LC. Both the kinases were found
305 to be heavily phosphorylated as 32 (MAK2-18, PMK3-14) phospho-peptides were detected.
306 We only show residues with probability of phosphorylation greater than 0.9 (Fig 3A-B). In
307 PMK3, six phosphorylated residues (T285, Y287, Y300, S347, T354, Y418) were located
308 within the kinase domain, while T107 was located just before the beginning of the kinase
309 domain, and S423 and S464 were situated after the kinase domain. In case of MAK2, three
310 residues (S148, T173, Y180) were located within the kinase domain, of which T173 and Y180
311 are situated in the activation loop of the kinase prior to the APE motif. No residue prior to the
312 kinase domain at the N-terminus was found to be phosphorylated in MAK2. T285, S290 and
313 S313 after the kinase domain were found to be phosphorylated of which S313 is positioned
314 within the nuclear export signal (NES) of MAK2. The TxY motif of PMK3 (T285-x-Y287) was
315 found to be phosphorylated in the reaction mixture strongly pointing to the ability of MAK2 to
316

activate PMK3 by a feedback mechanism. This result strongly suggests that activation of a central kinase like PMK3 can be achieved by both upstream kinase MKK4 (canonical activation) and/or downstream kinase MAK2 (noncanonical feedback activation).

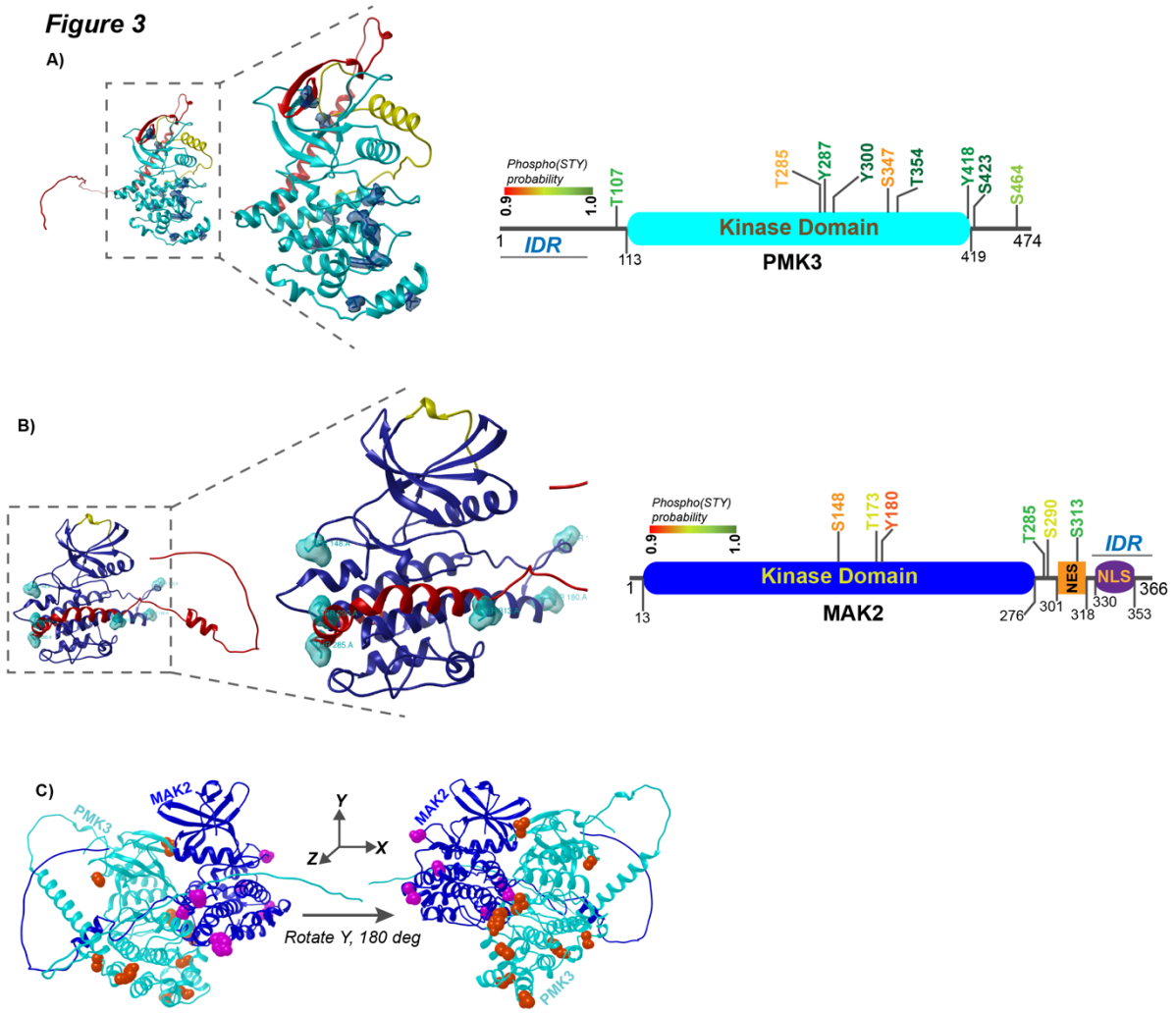


**Figure 3: Identification of phosphorylation sites on PMK3 and MAK2.**
**(A-B)** LC-MS/MS analysis reveals the amino acid residues phosphorylated on both these kinases in the feedback loop. (A) Right panel: Domain organization of PMK3 showing the identified phosphorylated residues. The residues have been colour coded as per the STY phosphorylation probability scale. Left panel: A zoomed in view of the AlphaFold predicted 3-D structure of PMK3, with the highlighted phosphorylation sites. (B) Right panel: Domain organization of MAK2 showing the identified phosphorylated residues. The residues have been colour coded as per the STY phosphorylation probability scale. Left panel: A zoomed in view of the AlphaFold predicted 3-D structure of MAK2, with the highlighted phosphorylation sites. **(C)** Distribution of the phospho-sites on distinct faces of the kinases points the dynamic nature of the PMK3:MAK2 complex with different possible modes of binding.

For both PMK3 and MAK2, we have depicted the phosphorylation sites in the context of the individual 3D-structures of these kinases. No experimentally derived three-dimensional structure of PMK3 or MAK2 is available in the database. For structural analyses we took

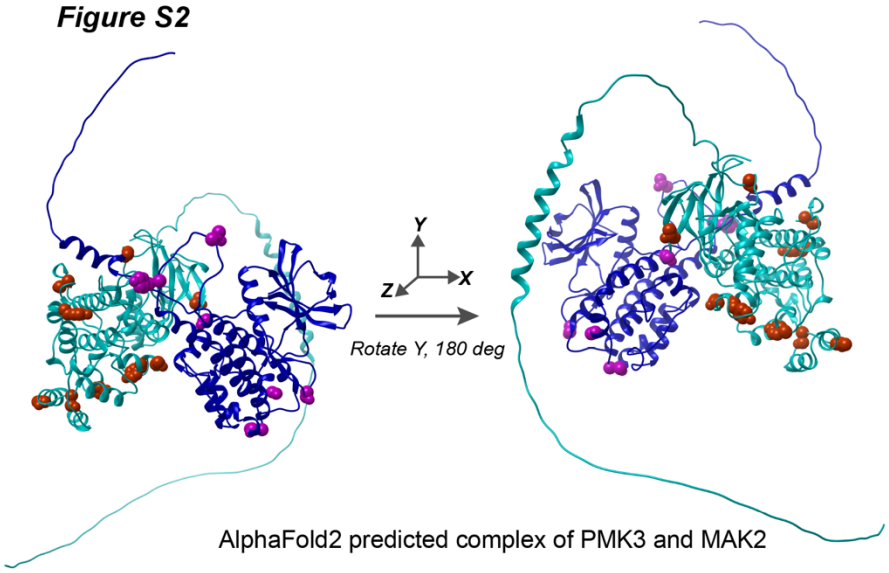


**Figure S2:** Ribbon representation of the AlphaFold2 predicted complex of PMK3 and MAK2. The phosphorylated residues identified by mass-spectrometric analyses have been highlighted (red and purple) on both the kinases.

advantage of the AlphaFold-predicted structures (Jumper et al., 2021) of these kinases. Closer look at the positions of phosphorylation sites on the 3D-structures of PMK3 and MAK2 revealed that they were dispersed on distinct faces of the kinases (Fig 3A- B). We further wanted to understand the implications of such distribution of phosphorylation sites in terms of the structure of the PMK3:MAK2 complex. However, no experimentally-derived structure of this complex is available in the literature. Firstly, we superimposed AlphaFold-derived structures of PMK3 and MAK2 on to the experimentally derived structure of the human p38$\alpha$:MK2 complex. When Phosphorylation sites on both PMK3 and MAK2 were highlighted it became clear that it was impossible for either kinase to access all the phosphorylation sites on the other kinase from this single pose (Fig 3C, left and right panels). Neither could these kinases autophosphorylate themselves at sites far from the respective active sites. We also created a model of the PMK3:MAK2 complex using AlphaFold2 and highlighted the phosphorylation sites (Fig S2). It was evident that this pose would not suffice to explain the distribution of phosphorylation sites on these two kinases either through trans-phosphorylation by each other or by self-phosphorylation. We surmised that PMK3:MAK2 complex is dynamic in nature that may exploit multiple mode of binding giving rise to an ensemble of conformations, and experimentally derived pose of the human p38$\alpha$:MK2 complex or AlphaFold2-derived PMK3:MAK2 complex are insufficient to capture the dynamicity of the said complex.

**Sequence and structural analyses of PMK3 and MAK2:**

Primary sequence of PMK3 was aligned with the four human p38 isoforms to reveal

that PMK3 shared highest sequence similarity with p38α (Fig S1B). We also subjected primary sequence of MAK2 to sequence alignment with three human MAPKAPKs, viz. MK2, MK3 and

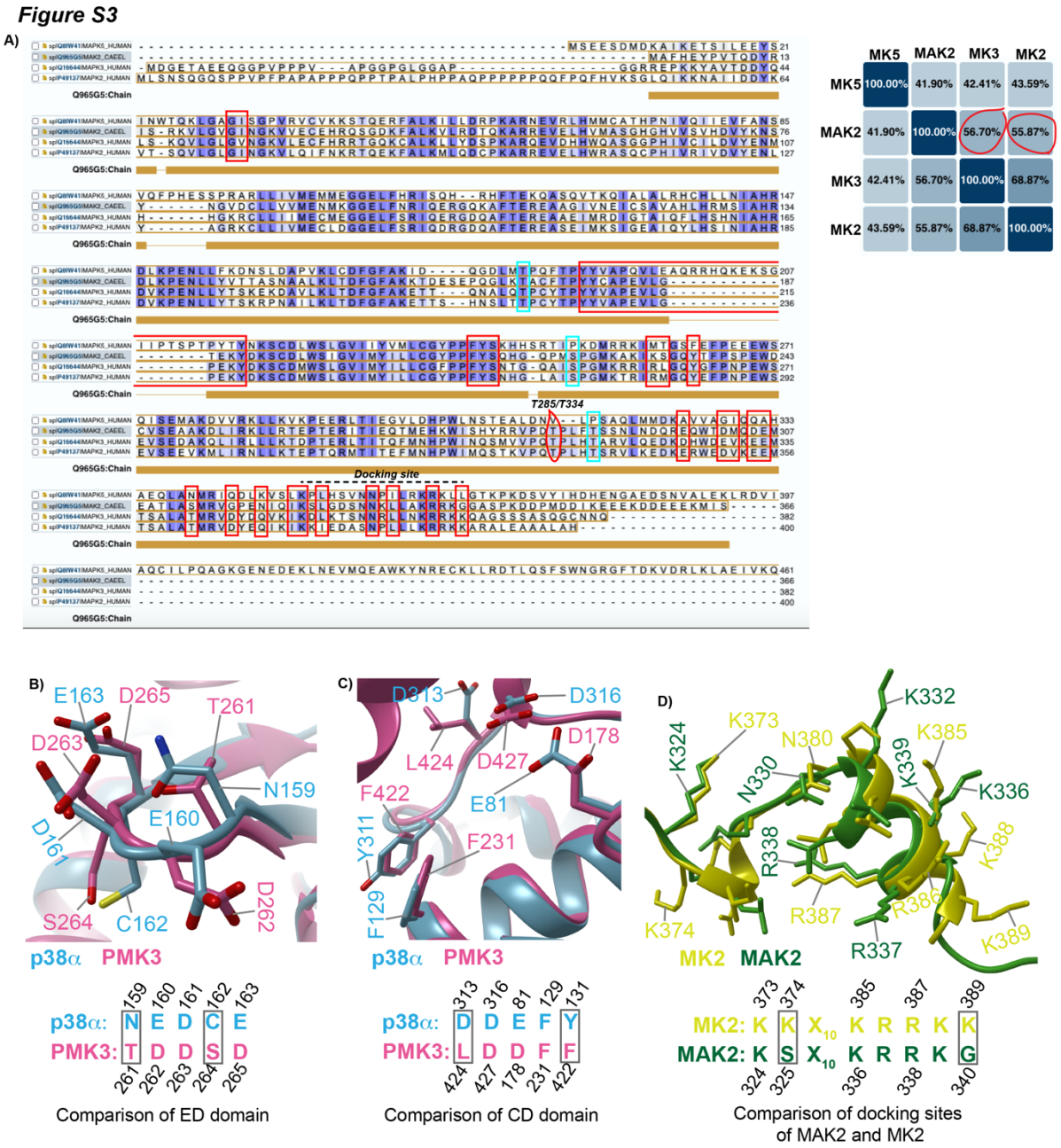


**Figure S3: (A)** Left panel: Multiple sequence alignment (MSA) of MAK2 with the human MAPKAPKs MK2, MK3 and MK5. Right panel: The percent identity matrix shows that MAK2 shares more than 50% sequence similarity with MK2 and MK3. **(B-C)** Superimposition of the ED and CD domains of PMK3 and human p38α. The respective sequence alignments have been shown in the lower panel. The changes in the nature of amino acids have been highlighted in boxes. **(D)** Superimposition of the docking sites of MAK2 and MK2 reveals that the involved residues are less conserved in MAK2 than in the human MKs.

MK5 (Fig S3A). It was found that, MAK2 shares more than 50% identity with two human MAPKAPKs, MK2 and MK3 (Fig S3A). In the context of binary complex between p38α and

368 MK2, we wanted to glean into the complex between PMK3 and MAK2. We superimposed the
369 respective kinases on the existing p38α:MK2 complex (pdb id: 2oza) and analyzed the regions
370 known to contribute to such complex formation. On the MAPK, there are two regions known
371 as CD and ED domains that contribute majorly to binding with the MAPKAPKs (Tanoue et al.,
372 2000; Tanoue et al., 2001). Fig S3B and S3C depict the superposition of ED and CD domains,
373 respectively along with their sequence alignment. Residues in the ED domain of these two
374 largely conserved with the exception of N159 of p38α changed to another polar residue T261
375 in PMK3, and C162 of p38α changed to S264 in PMK3 that merely changes -SH to -OH. In
376 the CD domain, however, changes are more drastic; acidic D313 of p38α changed to
377 hydrophobic L424 in PMK3 and polar, phosphorylatable Y131 of p38α changed to
378 hydrophobic, phospho-ablative F422 in PMK3. When we turned our attention to the p38-
379 docking site (R/K–R/K–$X_{10}$–R/K–R/K–R/K–R/K–R/K), we realized that this region of MAK2 is
380 not so conserved as compared to its human counterparts MK2 and MK3 (Fig S3D). For
381 example, 2$^{nd}$ R/K (K374 of MK2) and last R/K (K389 of MK2) have been changed to S325 and
382 G340, respectively in MAK2 (Fig S3D). Such changes in the interacting residues in the partner
383 kinases in the human and nematode raises the possibility that the ensuing PMK3:MAK2 may
384 not be exactly the same as the p38α:MK2 complex and they may differ in spatial arrangements
385 as well as affinity.
386 In the previous section we found out that the existing experimentally derived structural
387 models of human p38:MK2 structures and predicted PMK3:MAK2 structures were not
388 adequate to capture the nuances of the said complex of the nematode origin. We also found
389 out that the interacting residues are not entirely conserved in the nematode kinases. We
390 further noticed that PMK3 contains a long (~90aa) insert at the N-terminus before the kinase
391 domain that is absent in the human p38 isoforms. MAK2, on the other hand does not contain
392 any long N-terminal insertion before the beginning of the kinase domain that is present in MK2
393 and MK3 but not in MK5. MAK2, however has a highly charged C-terminal region beyond the
394 MAPK-docking sequence that is absent in MK2 or MK3. Both the N-terminal extension in
395 PMK3 and C-terminal extension in MAK2 are largely unstructured.
396 Such differences in their amino acid compositions prompted us to extensively analyze
397 those sequences using web-based tools to gain further insights on their physico-chemical
398 properties as presence of long IDRs entail possibility of condensate formation through liquid
399 liquid phase separation. We subjected both PMK3 and MAK2 sequences for such analyses
400 using multiple web-based tools to better understand the properties and outcomes of those
401 inserts before or after the well folded kinase domains present in them. We primarily used
402 MolPhase, FuzDrop, IUPred3, PONDR and FoldIndex webservers (Erdos et al., 2021; Hatos
403 et al., 2022; Liang et al., 2024; Prilusky et al., 2005). In Fig 4A, results of PMK3 sequence

analyses on MolPhase and FuzDrop are shown along with the AlphaFold-predicted structure colored according to the pLDDT scores that informs about the confidence of the prediction,

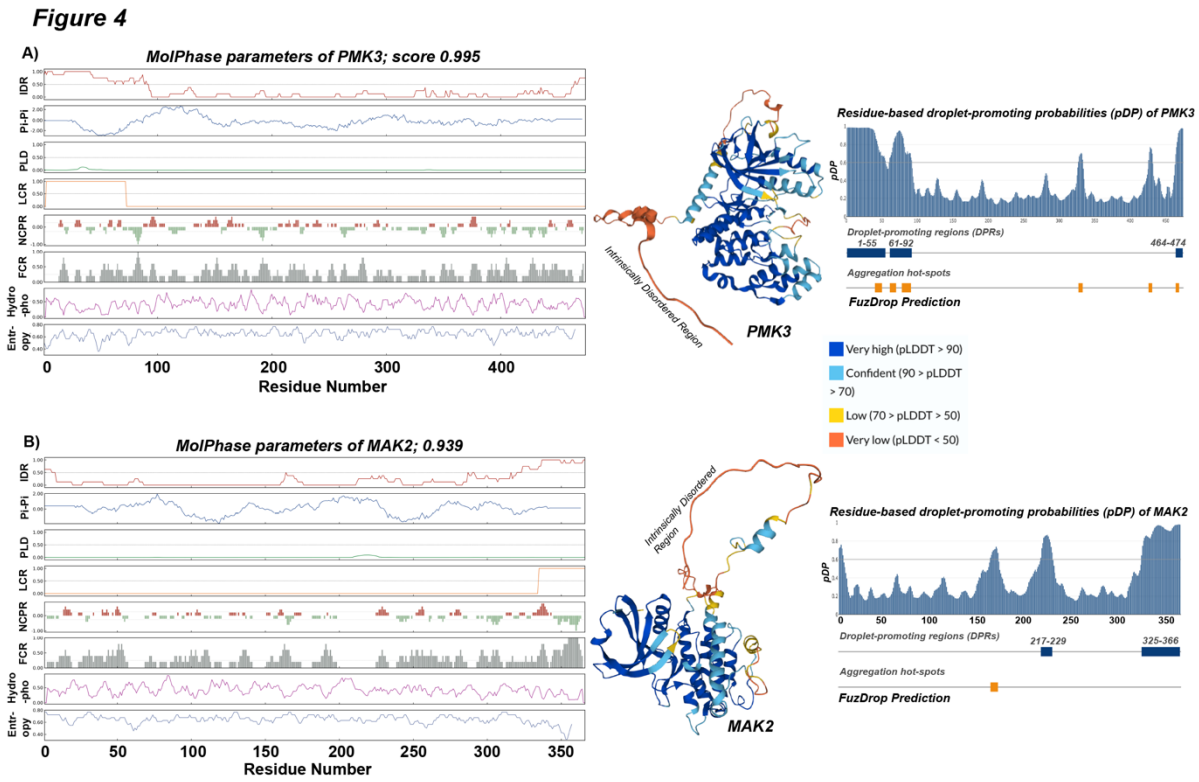


**Figure 4: PMK3 and MAK2 harbor unstructured, disordered regions and propensity to undergo phase separation**

**(A)** Left panel: MolPhase analysis of the primary sequence of PMK3 shows that the kinase consists of an intrinsically disordered region (IDR) at its N-terminus. Right panel: FuzDrop prediction shows the droplet promoting regions (DPRs) along with the aggregation hotspots in the PMK3 sequence. The AlphaFold predicted structure of PMK3 has been shown. The structural elements have been colour coded according to the pLDDT score that signifies the confidence of prediction. The data shows that the N-terminus of PMK3 forms a disordered region with a pLDDT score of less than 50. **(B)** Left panel: MolPhase and analysis of the primary sequence of MAK2 shows that the kinase consists of an intrinsically disordered region (IDR) in the middle (217-229) and at the C-terminus Right panel: FuzDrop prediction shows the droplet promoting regions (DPRs). The number of aggregation hot spots in the MAK2 sequence is distinctly lower than those found in PMK3.The AlphaFold predicted structure of MAK2 has been shown. The structural elements have been colour coded according to the pLDDT score that signifies the confidence of prediction. The data shows that the C-terminus of PMK3 forms a disordered and unstructured region with a pLDDT score of less than 50.

rest of the predictions are shown in Fig S4A. Similarly, prediction results for MAK2 are shown in Fig 4B and Fig S4B. It was observed in both cases, MolPhase and FuzDrop predictions correlated well with the AlphaFold prediction confidence score, i.e., pLDDT score (Jumper et al., 2021). For PMK3, the pLDDT score was lowest at the N-terminus prior to the kinase domain; the same region was predicted to be intrinsically disordered by each of the predictive

tools employed (Fig 4A and S4A). Similarly, MAK2 C-terminus beyond the kinase domain showed lowest confidence in the AlphaFold prediction that was also found to be intrinsically disordered by the predictive tools used in this study. Presence of intrinsically disordered regions (IDRs) bestow their parent protein with multivalency of interaction (Babu et al., 2011; Wright and Dyson, 2015). Since both PMK3 and MAK2 are found to contain long IDRs, it is possible that they would be capable of interacting with each other in multiple ways giving rise to an ensemble of intermolecular poses. It will posit residues of each kinase with respect to the active sites of the other kinase making phosphorylation of residues on opposite faces of the kinases plausible. Presence of IDRs also gives rise to the possibility of formation of molecular condensates through liquid liquid phase separation (LLPS). MolPhase score for PMK3 and MAK2 was 0.995 and 0.939, respectively strongly suggesting that these proteins are likely to form condensates through LLPS.

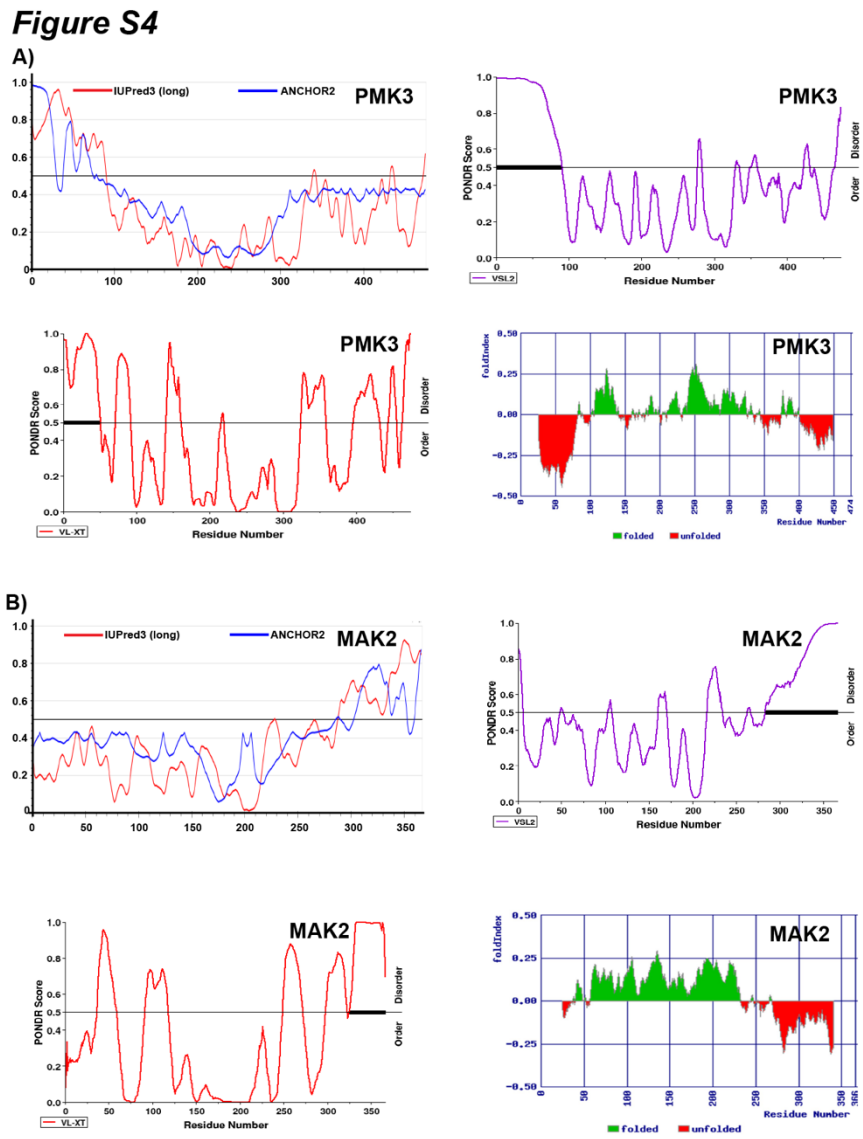


**Figure S4: (A-B)** IUPred3, PONDR and FoldIndex webserver-based predictions of PMK3 (A) and MAK2 (B) primary sequences.

**MAK2, but not PMK3, undergoes liquid-liquid phase separation:**

Analyses of the primary and AlphaFold predicted structure of MAK2 revealed the presence of a long intrinsically unstructured/disordered region (IDR) at the C-terminus of the

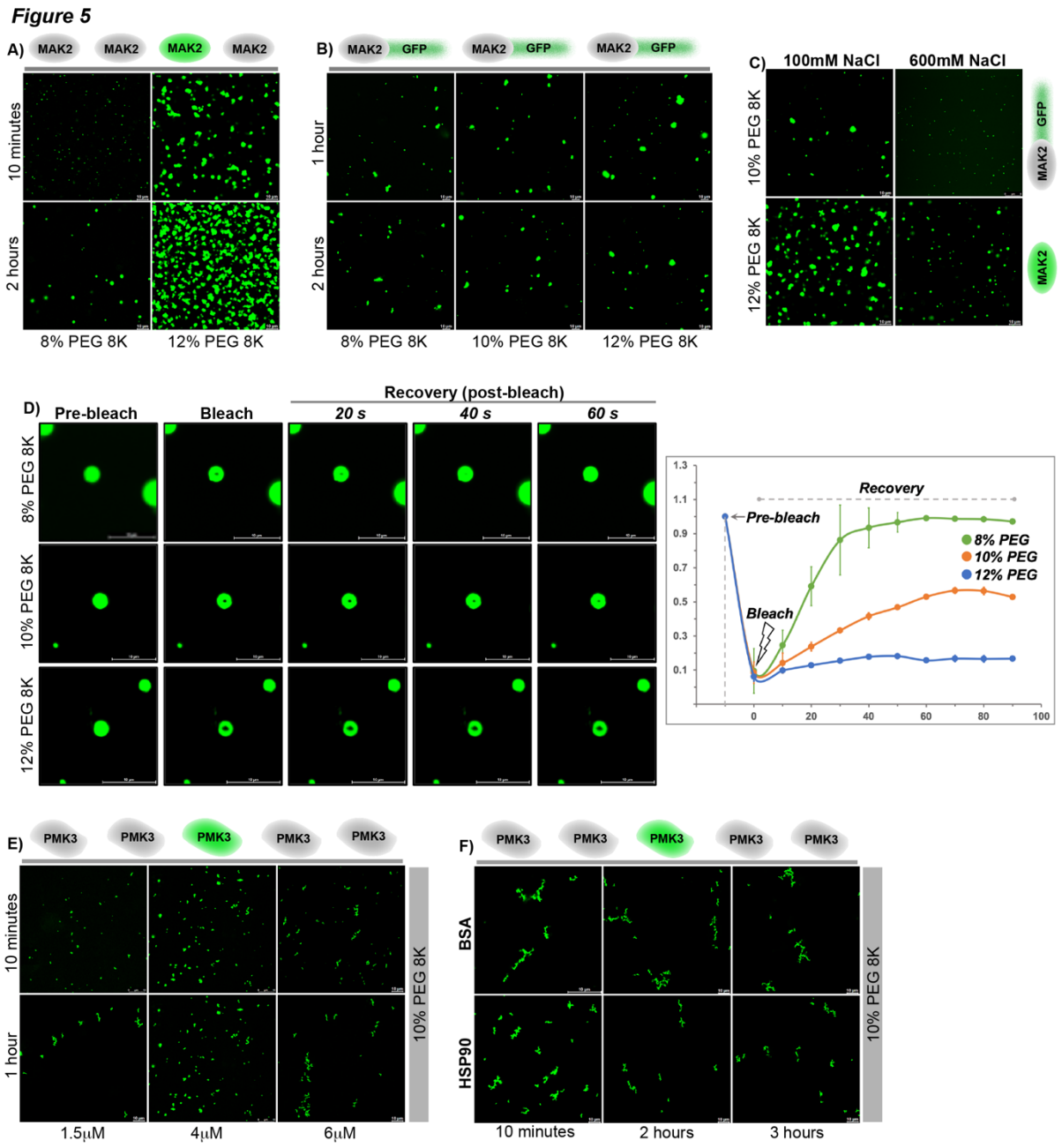


**Figure 5: MAK2 undergoes liquid- liquid phase separation (LLPS) to form condensates, whereas PMK3 forms aggregates.**

*In vitro* droplet formation assays. **(A)** Fluorescein labelled MAK2 was incubated with varying concentrations of PEG-8000 for different time periods and imaged under the microscope. MAK2 undergoes phase separation to form the round droplets under both the conditions. Images are representative of three independent experiments. Scale bar is 10μm. **(B)** A MAK2 construct with a GFP tag at its C-terminus (MAK2-GFP) could also successfully form these condensates through LLPS at the different PEG concentrations used. Images are representative of three independent experiments. Scale bar is 10μm **(C)** F-MAK2 and MAK2-GFP were subjected to phase separation in presence of increased amount of NaCl, wherein the droplet formation was significantly inhibited in both the cases at 600mM NaCl. Images are representative of two independent experiments. Scale bar is 8μm (upper panel) and 10μm (lower panel) respectively.

**(D)** FRAP analysis on the phase separated MAK2-GFP condensates at different PEG concentrations (left). Scale bar is 10μm.The fluorescence recovery in each case was followed up to 60 seconds post bleaching and the normalized fluorescence intensity was plotted against time (right). The data values are shown as mean±s.d. of normalized fluorescence intensity values from three independent measurements (n=3). **(E)** *In vitro* droplet formation assays with fluorescein labelled PMK3 show that PMK3 forms aggregates at different protein concentrations in the presence of 10% PEG-8K. Images are representative of three independent experiments. Scale bar is 10μm. **(F)** PMK3 forms aggregates even in the presence of chaperone Hsp90 or a non-specific interacting protein, BSA. Scale bar is 10μm.

protein with high probability of forming liquid droplets. LLPS-mediated condensate formation is a well-established mechanism to regulate a number of biological processes (Alberti and Dormann, 2019; Banani et al., 2017; Boeynaems et al., 2018; Franzmann and Alberti, 2019; Hyman et al., 2014; Peeples and Rosen, 2021; Posey et al., 2018). To test if MAK2 indeed forms droplets through liquid-liquid phase separation (LLPS) we prepared recombinant MAK2 labeled with Fluorescin (F-MAK2) and subjected it to treatment with varying concentration of PEG 8000 to drive phase separation at a MAK2 concentration of 10uM and 150mM NaCl. We found that MAK2 forms condensates through LLPS at concentration of PEG 8% and above (Fig 5A). It was observed that, with the increase in PEG concentration both the number and size of the condensates increased. At 12% PEG, the condensates seemed to be transitioning from a liquid-like state to an arrested state. To further confirm that LLPS in MAK2 was not due to the specific labeling of the protein with Fluorescin, we generated and purified a MAK2 construct containing GFP at its C-terminus (MAK2-GFP). MAK2-GFP protein also underwent LLPS to form condensate in a range of PEG concentration ranging from 8-12% (Fig 5B) (Chauhan et al., 2024). Next, we checked the effect of protein concentration on LLPS by treating different concentration of MAK2-GFP with a fixed concentration of PEG (10%) (Chauhan et al., 2024). This assay revealed that size of the condensates increased as protein concentration was increased from 6uM to 10uM or more (Fig S5A). To assess the liquid like properties of the condensates we performed FRAP experiments at different concentrations of PEG (Taylor et al., 2019). It was observed that the fluorescence fully recovered within 60s of bleaching at 8% PEG while it was gradually arrested as the PEG concentration was increased to 10% and 12% (Fig 5D). To assess if LLPS in MAK2 was irreversible or reversible in our experimental conditions, we subjected both F-MAK2 and MAK2-GFP to condensate formation through LLPS at different concentrations of NaCl (Krainer et al., 2021; Posey et al., 2018; Sanulli and Narlikar, 2021). It was observed that, LLPS of MAK2 was severely compromised at higher concentration of NaCl both in case of F-MAK2 and MAK2-GFP (Fig 5C). These observations indicate that MAK2 LLPS is a reversible process energetics of which is likely dominated by electrostatic interactions (Posey et al., 2018; Sanulli and Narlikar, 2021).

As mentioned earlier, analysis of PMK3 sequence using web-based tools also predicted to contain long droplet promoting regions at its N-terminus, and a small region at the

*Figure S5*

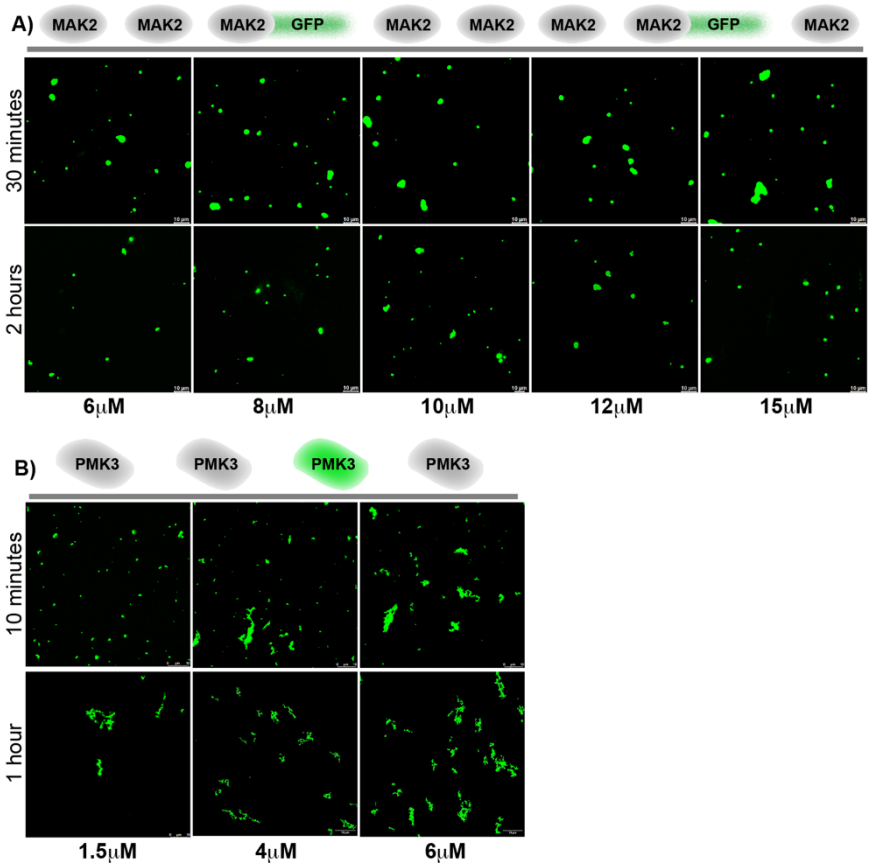


C-terminus. We wanted to check if PMK3 also formed droplets through LLPS. Recombinantly purified PMK3 was labeled with Fluorescin (F-PMK3). Different concentrations of F-PMK3 was incubated with different concentrations of PEG 8K to check for LLPS. It was observed that, F-PMK3 formed aggregates instead of phase-separated droplets at the protein

**Figure S5: (A)** Concentration dependent phase separation of MAK2-GFP in presence of 10% PEG. MAK2-GFP was mixed with 10% PEG at different protein concentrations up to 15μM and imaged under the microscope to check for visible droplet formation. Scale bar is 10μm. **(B)** F-PMK3 undergoes aggregation at different protein concentrations in the presence of 12% PEG-8K. Scale bar is 10μm.

concentrations tested in the same conditions that lead to LLPS-mediated droplet formation in MAK2 (Fig 5E and S5B). Furthermore, this aggregation of F-PMK3 could not be prevented by the chaperone HSP90 or a non-interacting non-specific protein, BSA (Fig 5F).

**MAK2 prevents aggregation and drives LLPS of PMK3:**

In the previous section we have seen that, PMK3 protein is aggregation prone that was refractory to the presence of HSP90 or a non-interacting protein. We also observed that PMK3 and MAK2 participate in a hitherto unreported feedback phosphorylation loop. Furthermore, MAK2 undergoes LLPS in presence of molecular crowders at different protein and PEG concentrations. Taken together, we sought out to investigate if MAK2 could prevent the aggregation of PMK3 and lead to LLPS-mediated droplet formation in PMK3. To this end, we took fixed concentration F-PMK3 and incubated it with 10% PEG 8K in absence or presence of increasing concentration of unlabeled MAK2, and monitored F-PMK3 droplet formation at different time interval. Interestingly, MAK2 was able to prevent aggregation of PMK3 and drove

*Figure 6*

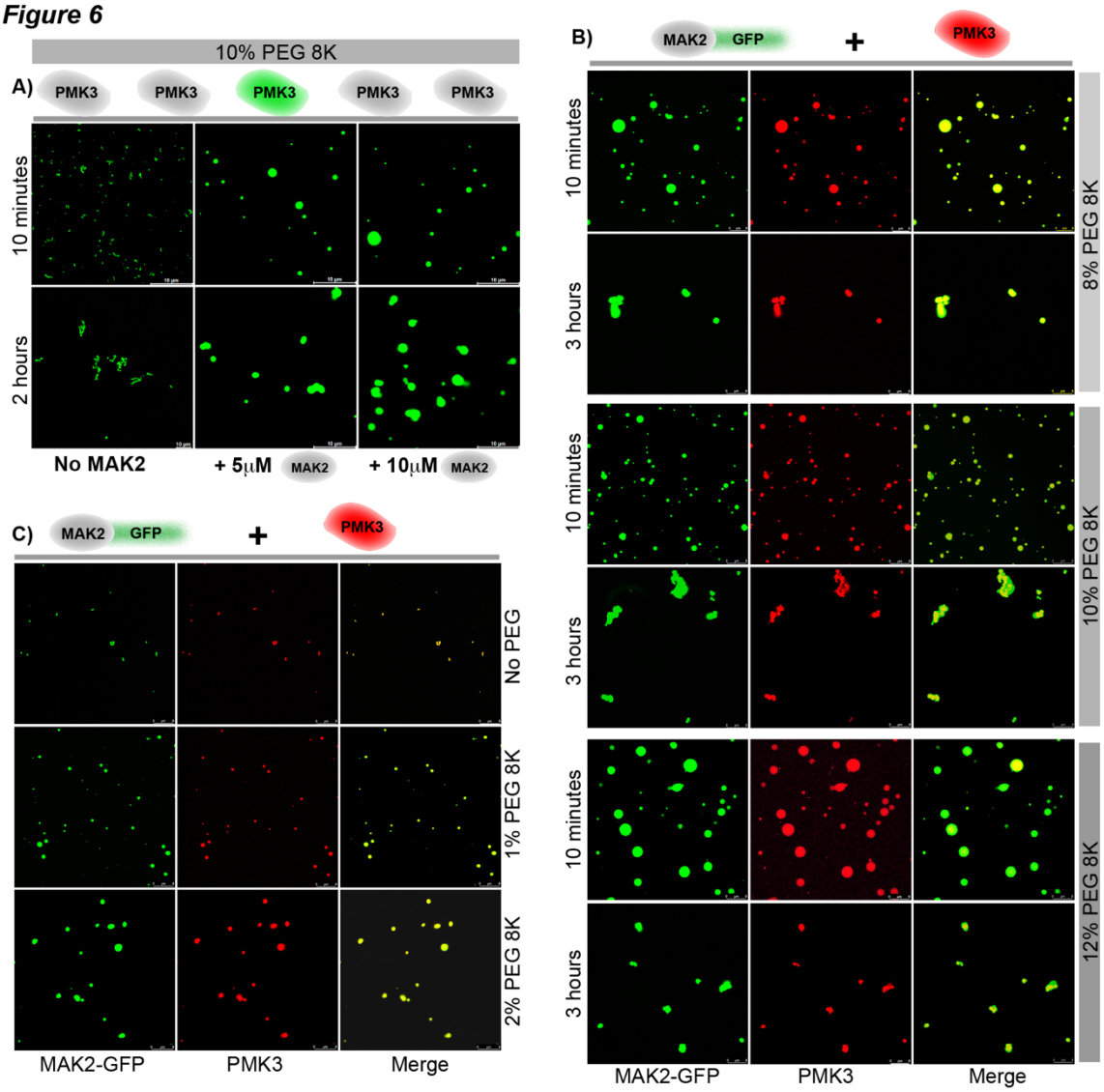


**Figure 6: MAK2 mediated phase separation prevents the aggregation of PMK3.** **(A)** F-PMK3 was mixed with unlabelled MAK2 at two different concentrations in presence of 10% PEG and imaged at 10 minutes and 2 hours respectively. In presence of MAK2, PMK3 undergoes liquid-liquid phase separation to form globular droplets instead of aggregates. Images are representative of two independent experiments. Scale bar is 10μm. **(B)** MAK2 and PMK3 co-localize within the same phase separated droplets. MAK-GFP (green) and Alexa 594 labelled PMK3 (red) were mixed together in presence of varying concentrations of PEG-8K (8-12%) and imaged at two time points. Merged (yellow) images show the co-localization of the two kinases within a single droplet. At 3 hours, the droplets exhibit a tendency to form aggregates with an increase in PEG concentration. Images are representative of two independent experiments. Scale bar is 8μm. **(C)** In presence of MAK2-GFP, PMK3 undergoes LLPS even in the absence of any crowding agent or as low as 1% PEG-8K. Scale bar is 8μm.

droplet formation in PMK3 through LLPS (Fig 6A). The above experiment proved that presence of MAK2 hinders aggregation pf PMK3 and induces LLPS-mediated droplet formation. Next, we asked whether this is a bystander-effect of MAK2 on PMK3. To this end, we wanted to see if the same droplets contain both MAK2 and PMK3. To distinguish between

560 the two under the microscope, we used MAK2-GFP and PMK3 was labeled Alexa Fluor 594
561 (AF-PMK3) for this study. AF-PMK3 and MAK2-GFP were mixed together and incubated in
562 presence of increasing concentration of PEG 8K for different time intervals before imaging.
563 We observed that, AF-PMK3 and MAK2-GFP colocalized in the same droplets in all the PEG
564 concentrations tested as early as 10 mins post incubation (Fig 6B). At 3 hours post incubation,
565 droplets showed tendency to aggregate with increasing concentration of PEG (Fig 6B).
566 Interestingly, AF-PMK3 and MAK2-GFP complex formed droplets through LLPS at PEG
567 concentration as low as 1-2%, very few droplets were seen even when no PEG was present
568 (Fig 6C).
569
570 **Effect of auto- and feedback phosphorylation on LLPS of the MAK2-PMK3 complex:**
571 It was evident from our biochemical analyses that MAK2 and PMK3 participate in a
572 feedback phosphorylation (trans-) loop whereas they undergo very little, if any, self-
573 phosphorylation when incubated alone with ATP. We wanted to see how these self- vs. trans-
574 phosphorylation modulate LLPS-mediated droplet formation and *vice-versa*. Firstly, we
575 wanted to compare the pan-phosphorylation abilities of PMK3 and MAK2 in LLPS-inducing
576 conditions. We employed two different reaction conditions, sets A and B, as outlined in Fig S6
577 (see materials and methods for further details). In set A, PMK3 was incubated alone in
578 presence of 10% PEG 8K that is known to cause aggregation of the kinase, and then MAK2
579 was added. In this condition, only the fraction of PMK3 that is available in solution or
580 condensate would serve as the kinase to phosphorylate MAK2 and as the substrate to be
581 phosphorylated by MAK2. In set B, PMK3 and MAK2 were incubated together in 10% PEG
582 8K. As we know, the PMK3:MAK2 complex will form condensate and a larger fraction of PMK3
583 should be biochemically available to serve as the kinase or the substrate. In our laboratory we
584 developed a non-hazardous, non-radioactive technique to detect this pan-phosphorylation
585 (*Borar et. al., unpublished data, manuscript in preparation*) using ATP-γ-S and PNBM followed
586 by detection of the p-thio-ester by immunoblotting using a specific antibody (Adler et al., 2013).
587 As expected, it was observed that in case of set A, phosphorylation signal for PMK3 was much
588 less as not much protein was available in solution/condensate even though catalytic amount
589 of PMK3 was available to allow phosphorylation of MAK2 (Fig 7A, left panel, lanes 1-3). In set
590 B, where PMK3:MAK2 complex was allowed to form the condensate both proteins underwent
591 significant phosphorylation (Fig 7A, left panel, lanes 4-6). We also checked if MAK2 was able
592 to phosphorylate PMK3 on tyrosine(s) when both were present in the condensate (set B).
593 Indeed, in the PMK3:MAK2 condensate MAK2 was able to phosphorylate tyrosine residue(s)
594 on PMK3 (Fig 7A, right panel) as was observed when both were present in solution (Fig 2H).
595 Next, MAK2-GFP was treated with ATP (200μM) and the mixture was incubated with crowding
596 agent and imaged at different time interval. When compared with the same protein in absence

*Figure 7*

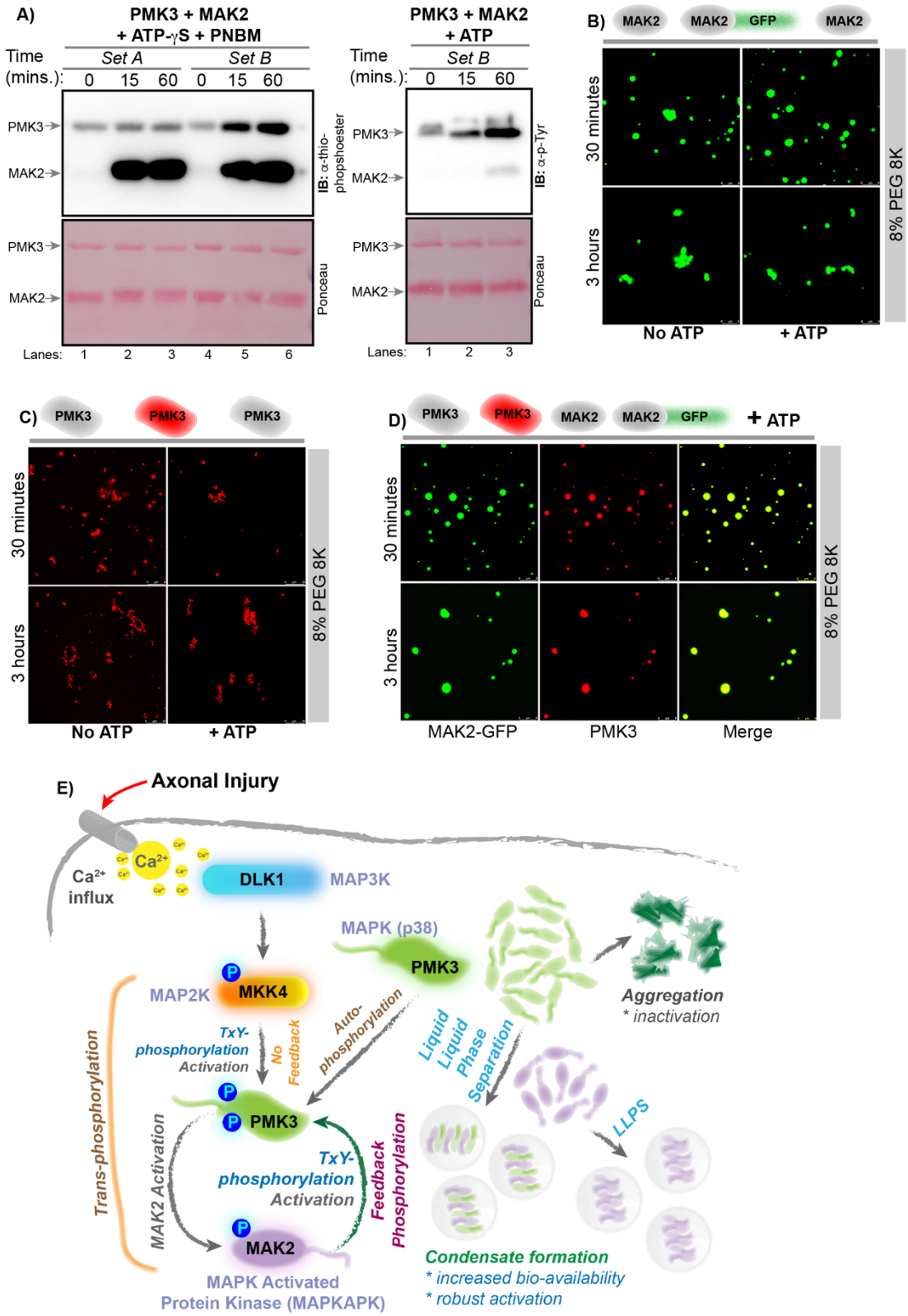


**Figure 7: Effect of auto- and feedback phosphorylation on LLPS of the MAK2-PMK3 complex.**

**(A)** MAK2 phosphorylates PMK3 on tyrosine residues within the condensates. PMK3 and MAK2 were incubated as per the reaction scheme in Figure S6, resolved by SDS-PAGE and probed using anti thio phosphate ester antibodies to detect the pan phosphorylation or anti p-tyrosine antibodies to detect phosphorylation at the tyrosine residues of the two kinases. Experiments were performed thrice with similar results.

**(B)** Effect of auto phosphorylation on the LLPS of MAK2. MAK2-GFP undergoes phase separation in the presence of ATP i.e. auto phosphorylation has no effect on the ability of MAK2 to form liquid condensates. Scale bar is 8µm. **(C)** Auto phosphorylated PMK3 forms aggregate in presence of 8% PEG-8K. Alexa 594 labelled PMK3 was used in this assay. Scale bar is 8µm. **(D)** Effect of trans-phosphorylation on PMK3: MAK2 condensates. Scale bar is 8µm. In presence of ATP, the PMK3: MAK2 droplets maintained their globular look even at 3 hours post incubation. (E) A graphical model depicting mutual relationship and signal transmission through PMK3 and MAK2. PMK3, a neuronal p38-MAPK is activated by its downstream MAPKAPK MAK2 without requiring the presence of canonical activator MAP2K, MKK4. MAK2 increases bioavailability of aggregation prone PMK3 by LLPS-driven condensate formation.

***Figure S6***

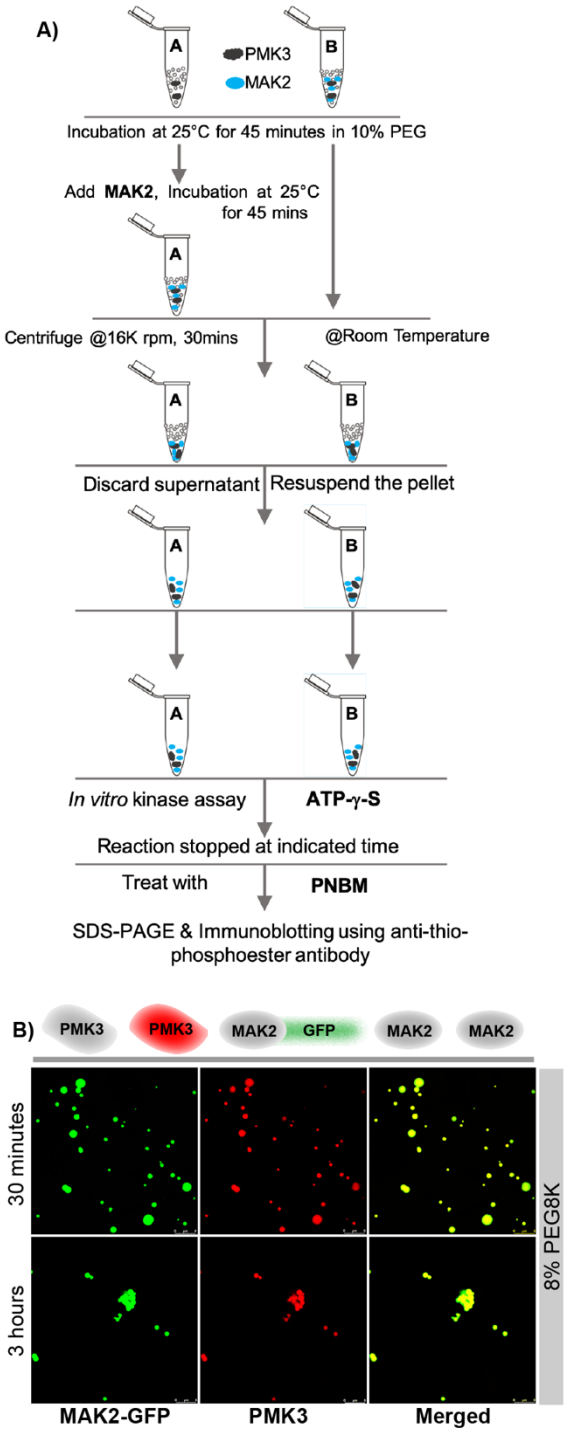


of ATP in the same assay condition they behaved similarly as to form droplets through LLPS (Fig 7B). We subjected AF-PMK3 to the same assay and found that presence of ATP did not change the fate to PMK3 to undergo aggregation as the AF-PMK3 alone in presence of the crowding agent (Fig 7C). Together these results inform us that autophosphorylation, if any, or

in other words mere presence of ATP is not sufficient to change PMK3's tendency to aggregate or MAK2's ability to from condensates through LLPS. Next, we incubated the MAK2-GFP and AF-PMK3 complex with crowding agent in presence and absence of ATP. MAK2:PMK3 complex underwent droplet formation through LLPS both in absence (Fig S6B), as was already seen, and presence of ATP (Fig 7D). Interestingly, we noticed that after prolonged incubation the complex also showed tendency to aggregate in absence of ATP but such a tendency to aggregate was not apparent in presence of ATP.

**Figure S6: (A)** Outline of the reaction schemes followed for the *in vitro* LLPS and their subsequent Western blot analyses using anti thio-phosphate ester and anti p-tyrosine antibodies. **(B)** Condensate formation of the PMK:MAK2 complex through LLPS in absence of ATP.

670 In presence of ATP the droplets generated through LLPS maintained their rounded-looks even
671 after 3hrs post-incubation. These results show that PMK3 might require the presence of MAK2
672 even in the presence of ATP that is abound in cellular milieu to remain bio-available in the
673 form of condensates along with MAK2, and that MAK2 is able to activate PMK3 in the
674 condensate state as well.

675 **Discussion:**

676 MAPK signaling modules have remained in the forefront of signal transduction
677 research for many years. A flood of research articles employing biochemical, structural,
678 genetics and other approaches helped the field to understand the importance of these kinases
679 and their regulatory mechanisms in great details (Cargnello and Roux, 2011; Chang and Karin,
680 2001; Goldsmith et al., 2010). Studies of MAPKs in multicellular (mammalian) and unicellular
681 (yeast) organisms show that they follow a unidirectional path starting from a MAP3K that
682 activates a cognate MAP2K to activate its downstream MAPK upon encountering extracellular
683 stimuli. Basic structure and skeleton of this three-kinase module is preserved wherein
684 MAP2Ks are dual specificity kinase required to phosphorylate the conserved TxY motif on the
685 activation loop of the MAPKs essential for the MAPKs to realize their full scale of activity
686 (Zhang et al., 2008). The three-kinase MAPK modules exhibit their roles either by directly
687 phosphorylating effector-substrates (like transcription factors) or by activating a downstream
688 kinase, MAPKAPK, by phosphorylation that ultimately carry out the phosphorylation of the
689 effector-substrates (Cargnello and Roux, 2011). This makes the module a four-kinase MAPK
690 module. Role of such MAPK-MAPKAPK duo are very well studied and well established in
691 literature and have been heavily implicated in mammalian biology especially in the realm of
692 immune signaling (Gaestel, 2006; Menon et al., 2017; Menon et al., 2018). Heterodimeric
693 p38$\alpha$:MK2 complex is known to orchestrate modulation of proinflammatory cytokine
694 productions (Menon and Gaestel, 2018). The complex is resident in the nucleus in resting
695 cells however migrates to the cytoplasm in response stimuli (Ben-Levy et al., 1998). p38$\alpha$
696 lacks NES however is transported to the cytoplasm in complex with MK2 that has an NES.
697 MK2-NES remains masked in its inactive form, phosphorylation (Thr334 in human) of NES by
698 p38$\alpha$ unmasks it (Ben-Levy et al., 1998; Engel et al., 1998; Meng et al., 2002).

699 As mentioned earlier, MAPK pathways represent one of the most ancient eukaryotic
700 signal transduction pathways throughout evolution. It is thus not surprising that they yet hold
701 many mysteries even though a great deal is already unearthed. For example, in *C. elegans*
702 PMK3 and MAK2 are greatly implicated in the axon regeneration pathway downstream of
703 DLK1 (MAP3K) and MKK4 (MAP2K) (Hammarlund et al., 2009; Yan et al., 2009). The DLK1
704 pathway is negatively regulated by the E3 ubiquitin ligase RPM-1/Highwire/Phr in worm, fly
705 and mice in order to stabilize the synaptic connections (Chang and Balice-Gordon, 2000;

706 Lewcock et al., 2007; Nakata et al., 2005; Schaefer et al., 2000). PMK3 and MAK2 were shown
707 to interact by yeast two hybrid assay and in a co-immunoprecipitation assay performed in
708 HEK293T cells (Yan et al., 2009). As expected PMK3 was able to phosphorylate MAK2 *in*
709 *vitro.* We found that, PMK3 tends to form large oligomeric forms in solution along with low
710 molecular weight fractions and that the oligomeric form is incapable of activating MAK2 by
711 phosphorylation. PMK3 phosphorylates MAK2 at T173 and Thr285 in addition to other
712 residues. It was shown that phospho-ablative double mutant of MAK2 (T173A T285A) failed
713 to exert its role in axonal regeneration in nematode (Yan et al Cell 2009). Thr285 in MAK2 is
714 equivalent to Thr334 in human MK2 located in the NES region, phosphorylation of which has
715 been well established in the activation and nuclear export of MK2 and p38$\alpha$:MK2 complex in
716 human to exert their signaling roles. Surprisingly, we found that the activated MAK2
717 phosphorylates PMK3 in return at multiple locations including the TxY (T285-x-Y287) motif
718 essential for PMK3 to attain its highest-activity state. This observation is unreported in the
719 literature, which proposes that MAK2 is actually a dual specificity kinase and not a Ser/Thr
720 kinase. Identification of phosphorylation site not only ascribes the novel specificity of MAK2, it
721 also provokes us to propose this newly found feedback loop as a mechanism that ascertain
722 the activation of a critical kinase like PMK3 by its downstream kinase in a situation when the
723 upstream MAP2K is absent/inactive. Of note, MK2 (mammalian counterpart of MAK2) has
724 been reported to participate in a feedback relationship with RIPK1 that downregulates RIPK1
725 activity (Menon et al., 2017; Menon et al., 2018). We speculate that the feedback loop either
726 may act as a fail-safe mechanism to activate PMK3 in a situation when MKK4 is either absent
727 or inactivated or it may help gain quicker and more robust response of this pathway as and
728 when required. Since DLK-1 signaling is used in multiple phenomena such as axon
729 regeneration (Hammarlund et al., 2009), degeneration (Asghari Adib et al., 2018; Gerdts et
730 al., 2016), and synaptic pruning (Asghari Adib et al., 2024) in response to nervous system
731 injury, it might need a fail-safe and seamless mechanisms for robust activation and faithful
732 transmission inside the cell. A critical dependence on two different P38 MAPK cascades
733 involving DLK-1 and MLK-1 for axonal regeneration, indicates a robust cross-talk between
734 parallel signaling kinases in neuronal injury response (Nix et al., 2011). Future course of
735 studies will shed light on the scenario in the cellular context in presence and absence of MKK4.
736 Phosphorylation mediated regulation of kinases is a common theme in kinase biology.
737 Distribution of phosphorylation sites on either kinase in this study suggested that the existing
738 structural models with similar kinases from other organisms were inadequate to capture the
739 possible modes of binding between PMK3 and MAK2 to enable such distribution of
740 phosphorylation sites. In addition, both these kinases contained IDRs and showed theoretical
741 propensity to form droplets. These observations led us to hypothesize that droplet/condensate
742 formation through LLPS might be a plausible mechanism to accommodate the ensemble

743 conformational space of this complex. In many cases, kinases have been found to depend
744 upon scaffolding proteins to undergo phosphorylation by a trans-kinase or to attain a critical
745 local concentration self-phosphorylation. Activation of IKK-complex is a classic example of
746 scaffolding protein (NEMO) dependent kinase (IKK) activation. It was recently shown that IKK-
747 complex undergo condensate formation through LLPS in the signaling context in a NEMO-
748 dependent manner (Du et al., 2022). Regulation of kinase function through LLPS-driven
749 condensate formation have been reported in many other cases as well (Lin et al., 2022; Lopez-
750 Palacios and Andersen, 2023; Sang et al., 2022; Schlutermann et al., 2021; Zhang et al.,
751 2020; Zhu et al., 2023). However, to the best of our knowledge, LLPS-mediated formation of
752 kinase-condensate that relies upon the presence of a trans-phosphorylating kinase is not
753 known. Here, for the first time we report that an aggregation-prone p38 MAPK (PMK3) is kept
754 bio-available by its activating downstream kinase MAPKAPK (MAK2) by formation of
755 condensates through LLPS. Furthermore, this LLPS-mediated condensate formation leads to
756 productive association between two kinases where the feedback phosphorylation relationship
757 is functional unlike the inactive oligomeric state. Interestingly, it has been shown recently that
758 human MKK6:p38$\alpha$ is also highly dynamic in nature and the disordered N-terminal linker of
759 the MAP2K (MKK6) plays critical role in determining specificity of the MAPK to be activated
760 by phosphorylation (Juyoux et al., 2023). This report and our observations provoke us to
761 speculate that MAPK activation across species might occur through a highly dynamical
762 engagement of the MAPK with its upstream (MAP2K) or downstream (MAPKAP) kinases with
763 ensuing conformational plasticity.
764 Together, we propose a hitherto unreported regulatory mechanism in kinases wherein
765 a critical signaling kinase is kept bio-available through LLPS by its downstream substrate
766 kinase that in turn activate the upstream kinase through a feedback phosphorylation loop (Fig
767 7E). Future course of studies will shed light whether this is a rare, kinase-specific mechanism
768 active in a particular organism or a more wide-spread aspect in kinase activation and
769 regulation.
770
771 **Materials and Methods:**
772 **Cloning of expression constructs:**
773 For large scale protein purification, the DNA encoding full length *C. elegans* PMK3 was
774 cloned within the EcoRI and XhoI restriction sites of a modified pET24d vector (pET24d-
775 HisTEV) designed to incorporate a N-terminal 6X His tag in the recombinant protein, followed
776 by a TEV protease cleavage site to remove the tag, if required. MAK2 was cloned within the
777 BamHI and SalI sites of pET24d-HisTEV. This plasmid consists of a kanamycin resistance
778 gene, a T7 promoter and a lacI coding sequence that allows for the IPTG-induced expression
779 of the cloned DNA. For the expression of GFP tagged MAK2, the insert was ligated to a

780 modified pET24d-HisTEV vector with a C-terminal GFP tag. The kinase dead PMK3 (K150M)
781 mutant was generated by site directed mutagenesis using Pfu DNA polymerase (Agilent). For
782 the purification of 6X His-MKK4 from Sf9-baculovirus expression system, the full-length
783 protein from *C. elegans* was cloned in pFastBacHT B vector at BamHI and XhoI restriction
784 sites. All the restriction enzymes and T4 DNA ligase were purchased from New England
785 Biolabs and ThermoFisher Scientific respectively.

786 **Culture growth conditions**

787 For recombinant protein expression, the plasmid constructs were transformed into *E.*
788 *coli* Rosetta 2 (DE3) strain. The transformants were selected on LB-agar plates supplemented
789 with 50µg/ml kanamycin. An overnight saturated culture of the transformed cells was used to
790 inoculate fresh Luria Bertani (LB) media supplemented with 50ug/ml of antibiotic kanamycin
791 (secondary culture) and incubated at 37°C up to an $OD_{600}$ of 0.5-0.6. The cells were then
792 induced with 0.25mM IPTG and grown overnight for 18-20 hours at 16°C, harvested by
793 centrifugation at 4500g and stored in -80°C until further processing.

794 **Protein purification from bacterial expression system**

795 For purifying the 6X His tagged recombinant proteins, bacterial cell pellet with
796 overexpressed protein of interest was re-suspended in a lysis buffer composed of 50mM Tris
797 pH 8.0, 200mM NaCl, 10mM imidazole, 10% glycerol, 5mM β-Me and 1mM freshly added
798 PMSF. Cells were lysed on ice using an ultra-sonic processor (Cole Parmer) and the crude
799 cell extract was clarified by centrifugation at 15000g for 1 hour. The supernatant was collected
800 and mixed with pre-equilibrated Ni-NTA agarose beads (Qiagen) at 4°C for 2 hours in batch
801 mode. The resin was washed with 10 CV (column volume) lysis buffer and 20 CV wash buffer
802 with 25mM imidazole. The bound protein was eluted with a buffer containing 50mM Tris pH
803 8.0, 200mM NaCl, 5% glycerol, 250mM imidazole, 5mM β-Me and 1mM PMSF. The protein
804 fractions were analysed by SDS-PAGE and stained with Coomassie Brilliant blue G-250
805 (Merck). The fractions with the desired protein were pooled together, filtered through a 0.22µm
806 filter and loaded on to a preparative HiLoad 16/600 Superdex 200 pg column (GE Healthcare),
807 connected to an ÄKTApure chromatography system (GE Healthcare), equilibrated with a
808 buffer consisting of 50mM Tris pH 8.0, 100mM NaCl, 3% glycerol, 5mM β-Me and 2mM EDTA.
809 The peak fractions were collected and run on SDS-PAGE. The proteins were further
810 concentrated, if required, using a 30kDa cut-off centrifugal protein concentrator (Vivaspin,
811 Sartorius). The final protein concentration was estimated using a microplate
812 spectrophotometer (Multiskan SkyHigh, Thermo Scientific) and the fractions were stored in -
813 80°C in small aliquots.

814 **Protein purification from Sf9-baculovirus expression system**

815 His-MKK4 was overexpressed in and purified from Sf9 (Thermo Scientific) cells.
816 Recombinant bacmid generation, transfection of the insect cells, generation and amplification

817 of recombinant baculovirus stock were done following the Bac-to-bac Baculovirus Expression
818 System user's manual (Thermo Scientific, MAN0000414). For large-scale purification, Sf9
819 cells in suspension at a cell density of 1X $10^6$ cells/ml were infected with P3 generation
820 baculoviruses and incubated at 27°C for 60-72 hours post-infection under shaking condition.
821 Cultures were harvested by centrifugation at 1200g for 30 minutes at 4°C, pellets were washed
822 with 1X TBS with 2mM EDTA and stored in -80°C. For protein purification, the cell pellets were
823 thawed, re-suspended in a lysis buffer containing 50mM Tris pH 8.0, 200mM NaCl, 10mM
824 imidazole, 10% glycerol, 5mM β-Me, 1mM PMSF and 1X protease inhibitor cocktail (Sigma-
825 Aldrich) and lysed on ice using sonication. The protein of interest was purified by Ni-NTA
826 affinity chromatography (as described above), followed by size exclusion chromatography
827 using a preparative HiLoad 16/600 Superdex 200 pg column (GE Healthcare) column. The
828 protein was eluted in a buffer containing 50mM Tris pH 8.0, 100mM NaCl, 3% glycerol, 5mM
829 β-Me and 2mM EDTA, concentrated using a centrifugal protein concentrator and stored in -
830 80°C in small aliquots.

831 ***In vitro* radioactive kinase assays**

832 *In vitro* radioactive kinase assays were performed to determine the functional status of
833 the purified recombinant kinases and to understand their mutual interactions. $\gamma^{32}$P-ATP was
834 used as the phosphor donor to detect the auto and trans phosphorylation events. Reactions
835 were carried out with the purified kinases, 200μM cold ATP mixed with $\gamma^{32}$P-ATP (hot ATP),
836 in presence of a kinase assay buffer composed of 20mM HEPES pH 7.7, 20mM β-
837 glycerophosphate, 100mM NaCl, 100μM sodium orthovanadate, 10mM $MgCl_2$, 10mM sodium
838 fluoride, 1mM PMSF and 2mM DTT (freshly added). The purified myelin basic protein (MBP)
839 used as a generic substrate was purchased from Sigma-Aldrich. All the reactions were
840 incubated at 25°C, up to different time intervals, terminated with 4X SDS protein loading dye,
841 boiled for 5 minutes at 100°C and resolved by SDS-PAGE. To confirm the amount of each
842 protein in the respective samples, the polyacrylamide gels were stained with Coomassie dye.
843 The Coomassie stained gels were subsequently dried using a gel drying equipment (Biorad
844 Model 583) and placed inside an exposure cassette (GE Healthcare). The phosphor signal
845 from each gel was captured on a phospho imager screen (GE Healthcare) and scanned using
846 an Amersham Typhoon Imager (GE Healthcare). The data was quantified using the ImageJ
847 software.

848 **Sample preparation for mass spectrometric analysis by LC-MS/MS**

849 To identify the residues phosphorylated on PMK3 and MAK2 by the feedback loop,
850 MS samples were prepared and analysed by LC-MS/MS. *In vitro* phosphorylation assay was
851 performed with cold ATP (200μM) in 1X kinase assay buffer using both proteins (30μg of
852 PMK3 and 100μg of MAK2). Reaction was incubated for 1 hour at 25°C. The sample was

853 passed through Zeba Spin de-salting columns (Thermo Scientific) and exchanged to a buffer
854 with 50mM ammonium bicarbonate and 5mM DTT (Promega). Resulting sample was
855 incubated at 56°C for 45 minutes, the final DTT concentration was subsequently adjusted to
856 10mM and further incubated for 15 minutes at 90°C. The reaction mixture was then cooled to
857 room temperature, and iodoacetamide (IAA; Promega) was added to a final concentration of
858 20mM and incubated for 1 hour at room temperature in the dark. 5mM DTT was further added
859 to the sample and incubated for another 30 minutes at room temperature neutralize excess
860 IAA in the reaction. The trypsin stock was prepared in 50mM ammonium bicarbonate and
861 added at a ratio of 1:100 (w/w). The added trypsin was diluted around 50-fold in the digestion
862 reaction by additional 50mM ammonium bicarbonate. The trypsin was added in two steps:
863 after the initial addition, the samples were incubated at 37°C for 1 hour, followed by the
864 addition of another round of trypsin and overnight incubation at 37°C. Reactions were stopped
865 with 0.1% trifluoroacetic acid (TFA) to reduce the pH below 4. The samples were vacuum-
866 dried in a SpeedVac (Thermo Scientific, Savant SPD111V) and the resulting peptides were
867 selectively enriched using the Thermo Fisher High-Select $TiO_2$ Phosphopeptide Enrichment
868 Kit (Cat. No A32993), following the manufacturer's instructions.
869 Digested peptides were desalted and enriched using Pierce C18 Tips (Thermo
870 Scientific). Eluted peptides were resuspended in 5% (v/v) formic acid and sonicated for 5 min.
871 Samples were analyzed on Orbitrap Exploris™ 240 mass spectrometer (Thermo Scientific)
872 coupled to a nanoflow LC system (Easy nLC II, Thermo Scientific). Peptide fractions were
873 loaded onto a PepMap™ RSLC C18 nanocapillary reverse phase HPLC column (75 µm × 25
874 cm; 2µm; 100 Å) and separated using a 60 min linear gradient of the organic mobile phase
875 [5% Acetonitrile (ACN) containing 0.1% formic acid and 95% ACN containing 0.1% formic
876 acid]. For identification of peptides the raw data was analyzed on MaxQuant proteomics
877 computational platform (Ver. 1.6.8) (Cox and Mann, 2008) and searched against UniProt
878 amino acid sequences (Uniprot ID: Q965G5; O44514) using phosphorylation (STY) as a
879 variable modification. The MS-based proteomics data of these experiments have been
880 deposited in the ProteomeXchange Consortium via the PRIDE partner repositiory with the
881 dataset identifier PXD054369 (Vizcaino et al., 2014).
882 **Fluorescent labelling of proteins**
883 Purified MAK2 was labelled with Fluorescein-5-Maleimide (Thermo Fisher Scientific)
884 for the fluorescent detection of the proteins under confocal microscope. The proteins were
885 prepared in a 20mM potassium phosphate buffer pH 7.2 with 100mM NaCl, 3% glycerol, 2mM
886 EDTA and 50µM TCEP. The fluorophore was added to the protein at a molar concentration
887 ratio of 8:1 and incubated on ice for 4-5 hours with intermittent mixing. The reaction was
888 terminated with 5mM DTT. The excess dye was removed using a PD SpinTrap G-25 (GE
889 Healthcare) desalting column and subsequent dialysis in 25mM Tris pH 8, 100mM NaCl, 3%

890 glycerol, 5mM β-Me and 1mM EDTA buffer. The samples were resolved by SDS-PAGE and
891 scanned in an Amersham Typhoon Imager (GE Healthcare) to confirm the labelling efficiency.
892 For PMK3, labelling was done with both Fluorescein-5-Maleimide (Thermo Fisher Scientific)
893 and Alexa Fluor 594 NHS Ester (Thermo Fisher Scientific). In case of Alexa Fluor 594, PMK3
894 was dialyzed against 20mM potassium phosphate buffer pH 8, 100mM NaCl, 3% glycerol,
895 5mM β-Me and 2mM EDTA and the protein to dye molar ratio was maintained at 1:5.

896 ***In vitro* droplet formation assay**

897 The *in vitro* LLPS of all proteins was performed either in presence of varying
898 concentrations of PEG-8000 (v/v) (Promega) or without any crowding agent in a dilution buffer
899 composed of 50mM Tris pH 8, 50mM NaCl, 2% glycerol, 5mM β-Me and 2mM EDTA. Proteins
900 in different concentrations/conditions were mixed with the desired amount of PEG-8000
901 solution and incubated at 25°C for different time periods. Liquid condensate or droplet
902 formation due to phase separation was followed by the visual turbidity of the samples and their
903 imaging in confocal microscope. 12µl of each sample was pipetted on to a glass slide and
904 covered with a cover slip for imaging. All fluorescent images were acquired using a Leica TCS
905 SP8 confocal microscope (63X oil immersion objective lens) or Leica Stellaris 5 laser scanning
906 microscope (100X oil immersion objective lens), equipped with SuiteX (Las X software).
907 Further image analyses were performed using the ImageJ software.

908 **Fluorescence recovery after photobleaching**

909 Fluidity and dynamics of the phase separated globular condensates were analysed
910 through FRAP. The FRAP experiments were performed on MAK2-GFP droplets within 20-30
911 minutes of the reaction initiation, using the FRAP module on the Leica microscope. Imaging
912 was performed using a 488nm laser for GFP at 100% power. 3 pre-bleach control images
913 were taken and subsequently a small circular ROI within a single droplet was bleached for 4
914 seconds. The fluorescence recovery within the bleached region was monitored for 90 seconds
915 post-bleaching (10seconds/frame). The fluorescence intensities at the post-bleach points
916 were normalized to the pre-bleach intensity and plotted to understand the degree of
917 fluorescence recovery.

918 ***In vitro* kinase assay using ATP-ɣ-S**

919 To monitor the de novo phosphorylation events involving the different kinases, *in vitro*
920 non-radioactive kinase assays were performed using the ATP analogue, ATP-ɣ-S (Enzo Life
921 Sciences). The LLPS samples under different conditions were incubated with 150µM ATP-ɣ-
922 S in a kinase assay buffer with 2mM TCEP and incubated at 25°C for the various mentioned
923 time points. Kinase reactions were quenched with 20mM EDTA. The proteins were then
924 alkylated with 1mM p-Nitrobenzyl mesylate (PNBM, Sigma Aldrich) and incubated further at
925 room temperature for 2 hours in the dark. Samples were subsequently boiled with SDS loading
926 dye and resolved by SDS-PAGE. The proteins were transferred on to PVDF membranes by

using semi-dry transfer apparatus. Blocking was done for 1 hour at room temperature with 5% BSA in TBS-T buffer, following which the membranes were incubated in the primary antibody (Thiophosphate Ester Specific RabMAb; Abcam) overnight at 4°C. An HRP-conjugated anti rabbit IgG (Thermo Fisher Scientific) was used as the secondary antibody. The protein bands were detected using enhanced chemi luminescence substrates (Thermo Scientific SuperSignal West Pico Chemiluminescent Substrate or Bio-Rad Clarity Western ECL substrate) in Amersham Imager 600.

**Immunoblotting using p-tyrosine antibodies**

To detect the pan-tyrosine phosphorylation on PMK3 and MAK2, kinase assays were set up with 200μM cold ATP in 1X kinase assay buffer and incubated at 25°C for the mentioned time intervals. Reactions were terminated with SDS loading dye, boiled at 100°C for 5 minutes, resolved by SDS-PAGE and subsequently transferred on to nitrocellulose or PVDF membranes. Following blocking for 1 hour in 5% BSA in TBS-T, the membranes were incubated in the specific p-tyrosine antibodies (BD Biosciences), overnight at 4°C. An HRP-conjugated anti mouse IgG (Thermo Fisher Scientific) was used as the secondary antibody.

**Kinetic Modelling:**

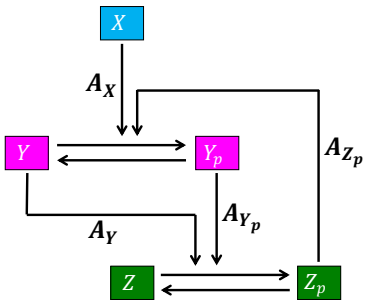


*Fig. 1 The Schematic of the phosphorelay kinetics of PMK3 (Y) and MAK2 (Z) mediated by MKK4 (X).*

The detailed kinetic steps of phosphorylation processes are the following:

$X$ mediated phosphorylation of $Y$ ($Y \xrightarrow{X} Y_p$)

$$\mathrm{Y} + X \underset{k_2^-}{\overset{k_2^+}{\rightleftarrows}} YX \xrightarrow{k_2} Y_p + X \tag{1}$$

$Z_p$ mediated phosphorylation of $Y$ ($Y \xrightarrow{Z_p} Y_p$)

$$\mathrm{Y} + Z_p \underset{k'^-_2}{\overset{k'^+_2}{\rightleftarrows}} YZ_p \xrightarrow{k'_2} Y_p + Z_p \tag{2}$$

$Y_p$ mediated phosphorylation of Z ($\mathrm{Z} \xrightarrow{Y_p} Z_p$)

$$\mathrm{Z} + Y_p \underset{k_3^-}{\overset{k_3^+}{\rightleftarrows}} ZY_p \overset{k_3}{\rightarrow} Z_p + Y_p \tag{3}$$

$Y$ mediated phosphorylation of $Z$ ($\mathrm{Z} \overset{Y}{\rightarrow} Z_p$)

$$\mathrm{Z} + Y \underset{k'^-_3}{\overset{k'^+_3}{\rightleftarrows}} ZY \overset{k'_3}{\rightarrow} Z_p + Y \tag{4}$$

We considered a Michaelis-Menten kinetic model, where the phosphorylation takes place through an intermediate complex formation, which either produce the phosphorylated form of the kinase or revert back to the unphosphorylated kinase form (Ferrell, 2022; Huang and Ferrell, 1996; Tian and Song, 2012). The respective rate constants for each kinetic steps are provided in the kinetic scheme (Eqs. (1-4)). We employ a coarse-grained approach for dephosphorylation processes ($Y_p \rightarrow Y$ and $Z_p \rightarrow Z$), assuming a direct conversion from the phosphorylated kinase back to the unphosphorylated kinase form. This simplification is appropriate when the focus lies on capturing the overall effect of phosphorylation kinetics on the larger network. We, now, formulate the system of coupled ordinary differential equations (CODEs) that describe the temporal evolution of each component considering both phosphorylation and the simplified dephosphorylation processes.

$$\frac{d[Y]}{dt} = -k_2^+[Y][X] + k_2^-[YX] - k_2'^+[Y]\left[Z_p\right] + k_2'^-\left[YZ_p\right] + k_{-2}\left[Y_p\right] - k_3'^+[Z][Y] + (k_3' + k_3'^-)[ZY] \tag{5}$$

$$\frac{d[Y_p]}{dt} = k_2[YX] + k_2'\left[YZ_p\right] - k_{-2}\left[Y_p\right] - k_3^+[Z]\left[Y_p\right] + (k_3 + k_3^-)[ZY_p] \tag{6}$$

$$\frac{d[Z]}{dt} = -k_3^+[Z]\left[Y_p\right] + k_3^-\left[ZY_p\right] - k_3'^+[Z][Y] + k_3'^-[ZY] + k_{-3}\left[Z_p\right] \tag{7}$$

$$\frac{d[Z_p]}{dt} = -k_2'^+[Y]\left[Z_p\right] + (k_2' + k_2'^-)\left[YZ_p\right] + k_3\left[ZY_p\right] + k_3'[ZY] - k_{-3}\left[Z_p\right] \tag{8}$$

$$\frac{d[YX]}{dt} = k_2^+[Y][X] - (k_2 + k_2^-)[YX] \tag{9}$$

$$\frac{d[YZ_p]}{dt} = k_2'^+[Y][Z_p] - (k_2' + k_2'^-)[YZ_p] \tag{10}$$

$$\frac{d[ZY_p]}{dt} = k_3^+[Z][Y_p] - (k_3 + k_3^-)[ZY_p] \tag{11}$$

$$\frac{d[ZY]}{dt} = k_3'^+[Z][Y] - (k_3' + k_3'^-)[ZY] \tag{12}$$

In the above CODEs, the rate constants for dephosphorylation of $Y_p$ and $Z_p$ are denoted as $k_{-2}$ and $k_{-3}$, respectively. We define the Michaelis-Menten constants for each phosphorylation steps (Eqs. (1-4)) as,

$$K_M^{(2)} = \frac{k_2 + k_2^-}{k_2^+}, K_M'^{(2)} = \frac{k_2' + k_2'^-}{k_2'^+}, K_M^{(3)} = \frac{k_3 + k_3^-}{k_3^+}, K_M'^{(3)} = \frac{k_3' + k_3'^-}{k_3'^+} \tag{13}$$

For $X$ regulated phosphorylation of $Y$ (Eq. (1)), we define a dimensionless parameter $A$, called activity of the corresponding regulatory molecule which modulate the phosphorylation process of the downstream kinase. Specifically, for $X$ mediated phosphorylation of $Y$ (Eq. (1)), we define the activity of $X$ as $A_X = k_2/K_M^{(2)}$. Similarly, for $Y_p$ mediated phosphorylation of $Z$ (Eq. (3)) activity of $Y_p$ is defined as $A_{Y_p} = k_3/K_M^{(3)}$ and for $Y$ mediated phosphorylation of $Z$ (Eq. (4)) activity of $Y$ is defined as $A_Y = k_3'/K_M'^{(3)}$. In the feedback loop where $Z_p$ induces phosphorylation of $Y$ (Eq. (2)), the activity of $Z_p$ is defined as $A_{Z_p} = k_2'/K_M'^{(2)}$. The activity, $A_{Z_p}$, also represents feedback sensitivity and strength (FSS). A higher value of $A_{Z_p}$ indicates stronger and more sensitive feedback regulation. Specifically, a higher $k_2'$ value increases the strength of feedback regulation, while a lower $K_M'^{(2)}$ value signifies higher sensitivity in the feedback regulation. In our model, we adjust the FSS ($A_{Z_p}$) to investigate the role of $Z_p$ feedback regulation in the dynamics of phosphorylation kinetics. The activities of the

regulators $X, Y$, and $Y_p$ ($A_X$, $A_Y$, and $A_{Y_p}$, respectively) can also be described in similar fashion in terms of regulatory sensitivity and strength.

**Parameters used:**

Total concentration of $X$, $[X] = 5\ \mu M$

Total concentration of $Y$, $[Y]_{\text{Total}} = 10\ \mu M$

Total concentration of $Z$, $[Z]_{\text{Total}} = 10\ \mu M$

Where,

$$[Y]_{total} = [Y] + [Y_p] + [YX] + [YZ_p] + [ZY_p] + [ZY]$$

$$[Z]_{total} = [Z] + [Z_p] + [YZ_p] + [ZY_p] + [ZY]$$

$$k_2^+ = 1.0\ \mu M^{-1}s^{-1}, k_2^- = 0.9\ s^{-1}, k_2 = 0.1\ s^{-1}, k_{-2} = 0.3\ s^{-1}$$

$$k_3^+ = 2.0\ \mu M^{-1}s^{-1}, k_3^- = 0.9\ s^{-1}, k_3 = 0.1\ s^{-1}, k_{-3} = 0.3\ s^{-1}$$

$$k_3'^+ = 0.1\ \mu M^{-1}s^{-1}, k_3'^- = 0.9\ s^{-1}, k_3' = 0.1\ s^{-1}$$

$$k_2'^- = 1.0\ s^{-1}, k_2' = 1.0\ s^{-1}$$

Based on these parameter values, the Michaelis-Menten constants take the values $K_M^{(2)} = 1\ \mu M$, $K_M^{(3)} = 0.5\ \mu M$, and $K_M'^{(3)} = 10\ \mu M$. Similarly, the activity values are, $A_X = 0.1$, $A_Y = 0.01$, and $A_{Y_p} = 0.2$.

We tune $k_2'^+$ so that $K_M'^{(2)} (= 1/k_2'^+)$ takes on different values allowing us to ultimately tune $A_{Z_p}$. This approach helps us explore how variations in FSS influence the phosphorylation kinetics.

**Acknowledgements and funding sources:** This study was primarily supported by an Intermediate Fellowship of the DBT-Wellcome Trust India Alliance (IA/I/15/1/501852) and intramural core funding from Bose Institute to SP. PR and AH thanks the University Grants Commission, Government of India, and SM thanks Bose Institute for graduate research fellowship. MN thanks Science and Engineering Research Board (GoI) for the National Post-doctoral fellowship (PDF/2022/001807). Authors thank Dr. Amitabha Majumdar (NCCS, Pune) for helpful discussion. Authors thank the proteomics facility at CSIR-CCMB for mass spectrometric data collection.

**Author contribution:**

Conceptualization: SP; Experimental design: SP and PR; Investigation: PR, PRT, AH, SM (structural modeling) and MN (kinetic modeling); Data analysis: SP, PR, AGR, SRC, PRT; Figure: SP, PR, PRT, MN, SM; First draft: SP; Editing: PR, AGR, PRT, MN

**Competing interests:** Authors declare no competing financial interests.

## References


Adler, J.J., Johnson, D.E., Heller, B.L., Bringman, L.R., Ranahan, W.P., Conwell, M.D., Sun, Y., Hudmon, A., and Wells, C.D. (2013). Serum deprivation inhibits the transcriptional co-activator YAP and cell growth via phosphorylation of the 130-kDa isoform of Angiomotin by the LATS1/2 protein kinases. Proc Natl Acad Sci U S A *110*, 17368-17373.

Alberti, S., and Dormann, D. (2019). Liquid-Liquid Phase Separation in Disease. Annu Rev Genet *53*, 171-194.

Asghari Adib, E., Shadrach, J.L., Reilly-Jankowiak, L., Dwivedi, M.K., Rogers, A.E., Shahzad, S., Passino, R., Giger, R.J., Pierchala, B.A., and Collins, C.A. (2024). DLK signaling in axotomized neurons triggers complement activation and loss of upstream synapses. Cell Rep *43*, 113801.

Asghari Adib, E., Smithson, L.J., and Collins, C.A. (2018). An axonal stress response pathway: degenerative and regenerative signaling by DLK. Curr Opin Neurobiol *53*, 110-119.

Babu, M.M., van der Lee, R., de Groot, N.S., and Gsponer, J. (2011). Intrinsically disordered proteins: regulation and disease. Curr Opin Struct Biol *21*, 432-440.

Banani, S.F., Lee, H.O., Hyman, A.A., and Rosen, M.K. (2017). Biomolecular condensates: organizers of cellular biochemistry. Nat Rev Mol Cell Biol *18*, 285-298.

Battagello, D.S., Dragunas, G., Klein, M.O., Ayub, A.L.P., Velloso, F.J., and Correa, R.G. (2020). Unpuzzling COVID-19: tissue-related signaling pathways associated with SARS-CoV-2 infection and transmission. Clin Sci (Lond) *134*, 2137-2160.

Ben-Levy, R., Hooper, S., Wilson, R., Paterson, H.F., and Marshall, C.J. (1998). Nuclear export of the stress-activated protein kinase p38 mediated by its substrate MAPKAP kinase-2. Curr Biol *8*, 1049-1057.

Berman, K., McKay, J., Avery, L., and Cobb, M. (2001). Isolation and characterization of pmk-(1-3): three p38 homologs in Caenorhabditis elegans. Mol Cell Biol Res Commun *4*, 337-344.

Boeynaems, S., Alberti, S., Fawzi, N.L., Mittag, T., Polymenidou, M., Rousseau, F., Schymkowitz, J., Shorter, J., Wolozin, B., Van Den Bosch, L.*, et al.* (2018). Protein Phase Separation: A New Phase in Cell Biology. Trends Cell Biol *28*, 420-435.

Bouhaddou, M., Memon, D., Meyer, B., White, K.M., Rezelj, V.V., Correa Marrero, M., Polacco, B.J., Melnyk, J.E., Ulferts, S., Kaake, R.M.*, et al.* (2020). The Global Phosphorylation Landscape of SARS-CoV-2 Infection. Cell *182*, 685-712 e619.

Canovas, B., and Nebreda, A.R. (2021). Diversity and versatility of p38 kinase signalling in health and disease. Nat Rev Mol Cell Biol *22*, 346-366.

Cargnello, M., and Roux, P.P. (2011). Activation and function of the MAPKs and their substrates, the MAPK-activated protein kinases. Microbiol Mol Biol Rev *75*, 50-83.

Chang, L., and Karin, M. (2001). Mammalian MAP kinase signalling cascades. Nature *410*, 37-40.

Chang, Q., and Balice-Gordon, R.J. (2000). Highwire, rpm-1, and futsch: balancing synaptic growth and stability. Neuron *26*, 287-290.

Chauhan, G., Bremer, A., Dar, F., Mittag, T., and Pappu, R.V. (2024). Crowder titrations enable the quantification of driving forces for macromolecular phase separation. Biophys J *123*, 1376-1392.

Cicirelli, M.F., Pelech, S.L., and Krebs, E.G. (1988). Activation of multiple protein kinases during the burst in protein phosphorylation that precedes the first meiotic cell division in Xenopus oocytes. J Biol Chem *263*, 2009-2019.

Cox, J., and Mann, M. (2008). MaxQuant enables high peptide identification rates, individualized p.p.b.-range mass accuracies and proteome-wide protein quantification. Nat Biotechnol *26*, 1367-1372.

Cuadrado, A., and Nebreda, A.R. (2010). Mechanisms and functions of p38 MAPK signalling. Biochem J *429*, 403-417.

Du, M., Ea, C.K., Fang, Y., and Chen, Z.J. (2022). Liquid phase separation of NEMO induced by polyubiquitin chains activates NF-kappaB. Mol Cell *82*, 2415-2426 e2415.

1073 Engel, K., Kotlyarov, A., and Gaestel, M. (1998). Leptomycin B-sensitive nuclear export of
1074 MAPKAP kinase 2 is regulated by phosphorylation. EMBO J *17*, 3363-3371.
1075 Erdos, G., Pajkos, M., and Dosztanyi, Z. (2021). IUPred3: prediction of protein disorder
1076 enhanced with unambiguous experimental annotation and visualization of evolutionary
1077 conservation. Nucleic Acids Res *49*, W297-W303.
1078 Ferrell, J.E., Jr. (2022). Systems Biology of Cell Signaling: Recurring Themes and
1079 Quantitative Models (Boca Raton: CRC Press).
1080 Franzmann, T.M., and Alberti, S. (2019). Protein Phase Separation as a Stress Survival
1081 Strategy. Cold Spring Harb Perspect Biol *11*.
1082 Gaestel, M. (2006). MAPKAP kinases - MKs - two's company, three's a crowd. Nat Rev Mol
1083 Cell Biol *7*, 120-130.
1084 Ge, B., Gram, H., Di Padova, F., Huang, B., New, L., Ulevitch, R.J., Luo, Y., and Han, J.
1085 (2002). MAPKK-independent activation of p38alpha mediated by TAB1-dependent
1086 autophosphorylation of p38alpha. Science *295*, 1291-1294.
1087 Gerdts, J., Summers, D.W., Milbrandt, J., and DiAntonio, A. (2016). Axon Self-Destruction:
1088 New Links among SARM1, MAPKs, and NAD+ Metabolism. Neuron *89*, 449-460.
1089 Goldsmith, E.J., Min, X., He, H., and Zhou, T. (2010). Structural studies of MAP Kinase
1090 cascade components. Methods Mol Biol *661*, 223-237.
1091 Hammarlund, M., Nix, P., Hauth, L., Jorgensen, E.M., and Bastiani, M. (2009). Axon
1092 regeneration requires a conserved MAP kinase pathway. Science *323*, 802-806.
1093 Han, J., Lee, J.D., Jiang, Y., Li, Z., Feng, L., and Ulevitch, R.J. (1996). Characterization of
1094 the structure and function of a novel MAP kinase kinase (MKK6). J Biol Chem *271*, 2886-
1095 2891.
1096 Hao, Y., Frey, E., Yoon, C., Wong, H., Nestorovski, D., Holzman, L.B., Giger, R.J.,
1097 DiAntonio, A., and Collins, C. (2016). An evolutionarily conserved mechanism for cAMP
1098 elicited axonal regeneration involves direct activation of the dual leucine zipper kinase DLK.
1099 Elife *5*.
1100 Hatos, A., Tosatto, S.C.E., Vendruscolo, M., and Fuxreiter, M. (2022). FuzDrop on
1101 AlphaFold: visualizing the sequence-dependent propensity of liquid-liquid phase separation
1102 and aggregation of proteins. Nucleic Acids Res *50*, W337-W344.
1103 Huang, C.Y., and Ferrell, J.E., Jr. (1996). Ultrasensitivity in the mitogen-activated protein
1104 kinase cascade. Proc Natl Acad Sci U S A *93*, 10078-10083.
1105 Hyman, A.A., Weber, C.A., and Julicher, F. (2014). Liquid-liquid phase separation in biology.
1106 Annu Rev Cell Dev Biol *30*, 39-58.
1107 Jumper, J., Evans, R., Pritzel, A., Green, T., Figurnov, M., Ronneberger, O.,
1108 Tunyasuvunakool, K., Bates, R., Zidek, A., Potapenko, A.*, et al.* (2021). Highly accurate
1109 protein structure prediction with AlphaFold. Nature *596*, 583-589.
1110 Juyoux, P., Galdadas, I., Gobbo, D., von Velsen, J., Pelosse, M., Tully, M., Vadas, O.,
1111 Gervasio, F.L., Pellegrini, E., and Bowler, M.W. (2023). Architecture of the MKK6-p38alpha
1112 complex defines the basis of MAPK specificity and activation. Science *381*, 1217-1225.
1113 Krainer, G., Welsh, T.J., Joseph, J.A., Espinosa, J.R., Wittmann, S., de Csillery, E., Sridhar,
1114 A., Toprakcioglu, Z., Gudiskyte, G., Czekalska, M.A.*, et al.* (2021). Reentrant liquid
1115 condensate phase of proteins is stabilized by hydrophobic and non-ionic interactions. Nat
1116 Commun *12*, 1085.
1117 Lewcock, J.W., Genoud, N., Lettieri, K., and Pfaff, S.L. (2007). The ubiquitin ligase Phr1
1118 regulates axon outgrowth through modulation of microtubule dynamics. Neuron *56*, 604-620.
1119 Liang, Q., Peng, N., Xie, Y., Kumar, N., Gao, W., and Miao, Y. (2024). MolPhase, an
1120 advanced prediction algorithm for protein phase separation. EMBO J *43*, 1898-1918.
1121 Lin, C.C., Suen, K.M., Jeffrey, P.A., Wieteska, L., Lidster, J.A., Bao, P., Curd, A.P.,
1122 Stainthorp, A., Seiler, C., Koss, H.*, et al.* (2022). Receptor tyrosine kinases regulate signal
1123 transduction through a liquid-liquid phase separated state. Mol Cell *82*, 1089-1106 e1012.
1124 Lopez-Palacios, T.P., and Andersen, J.L. (2023). Kinase regulation by liquid-liquid phase
1125 separation. Trends Cell Biol *33*, 649-666.

Luecke, S., Guo, X., Sheu, K.M., Singh, A., Lowe, S.C., Han, M., Diaz, J., Lopes, F., Wollman, R., and Hoffmann, A. (2024). Dynamical and combinatorial coding by MAPK p38 and NFkappaB in the inflammatory response of macrophages. Mol Syst Biol.

Manning, G., Plowman, G.D., Hunter, T., and Sudarsanam, S. (2002). Evolution of protein kinase signaling from yeast to man. Trends Biochem Sci *27*, 514-520.

Meng, W., Swenson, L.L., Fitzgibbon, M.J., Hayakawa, K., Ter Haar, E., Behrens, A.E., Fulghum, J.R., and Lippke, J.A. (2002). Structure of mitogen-activated protein kinase-activated protein (MAPKAP) kinase 2 suggests a bifunctional switch that couples kinase activation with nuclear export. J Biol Chem *277*, 37401-37405.

Menon, M.B., and Gaestel, M. (2018). MK2-TNF-Signaling Comes Full Circle. Trends Biochem Sci *43*, 170-179.

Menon, M.B., Gropengiesser, J., Fischer, J., Novikova, L., Deuretzbacher, A., Lafera, J., Schimmeck, H., Czymmeck, N., Ronkina, N., Kotlyarov, A.*, et al.* (2017). p38(MAPK)/MK2-dependent phosphorylation controls cytotoxic RIPK1 signalling in inflammation and infection. Nat Cell Biol *19*, 1248-1259.

Menon, M.B., Gropengiesser, J., Ruckdeschel, K., and Gaestel, M. (2018). To die or not to die: Regulatory feedback phosphorylation circuits determine receptor-interacting protein kinase-1 (RIPK1) function. Mol Cell Oncol *5*, e1396389.

Moriguchi, T., Kuroyanagi, N., Yamaguchi, K., Gotoh, Y., Irie, K., Kano, T., Shirakabe, K., Muro, Y., Shibuya, H., Matsumoto, K.*, et al.* (1996a). A novel kinase cascade mediated by mitogen-activated protein kinase kinase 6 and MKK3. J Biol Chem *271*, 13675-13679.

Moriguchi, T., Toyoshima, F., Gotoh, Y., Iwamatsu, A., Irie, K., Mori, E., Kuroyanagi, N., Hagiwara, M., Matsumoto, K., and Nishida, E. (1996b). Purification and identification of a major activator for p38 from osmotically shocked cells. Activation of mitogen-activated protein kinase kinase 6 by osmotic shock, tumor necrosis factor-alpha, and H2O2. J Biol Chem *271*, 26981-26988.

Nakata, K., Abrams, B., Grill, B., Goncharov, A., Huang, X., Chisholm, A.D., and Jin, Y. (2005). Regulation of a DLK-1 and p38 MAP kinase pathway by the ubiquitin ligase RPM-1 is required for presynaptic development. Cell *120*, 407-420.

Nix, P., Hisamoto, N., Matsumoto, K., and Bastiani, M. (2011). Axon regeneration requires coordinate activation of p38 and JNK MAPK pathways. Proc Natl Acad Sci U S A *108*, 10738-10743.

Pearson, G., Robinson, F., Beers Gibson, T., Xu, B.E., Karandikar, M., Berman, K., and Cobb, M.H. (2001). Mitogen-activated protein (MAP) kinase pathways: regulation and physiological functions. Endocr Rev *22*, 153-183.

Peeples, W., and Rosen, M.K. (2021). Mechanistic dissection of increased enzymatic rate in a phase-separated compartment. Nat Chem Biol *17*, 693-702.

Posey, A.E., Holehouse, A.S., and Pappu, R.V. (2018). Phase Separation of Intrinsically Disordered Proteins. Methods Enzymol *611*, 1-30.

Prilusky, J., Felder, C.E., Zeev-Ben-Mordehai, T., Rydberg, E.H., Man, O., Beckmann, J.S., Silman, I., and Sussman, J.L. (2005). FoldIndex: a simple tool to predict whether a given protein sequence is intrinsically unfolded. Bioinformatics *21*, 3435-3438.

Sang, D., Shu, T., Pantoja, C.F., Ibanez de Opakua, A., Zweckstetter, M., and Holt, L.J. (2022). Condensed-phase signaling can expand kinase specificity and respond to macromolecular crowding. Mol Cell *82*, 3693-3711 e3610.

Sanulli, S., and Narlikar, G.J. (2021). Generation and Biochemical Characterization of Phase-Separated Droplets Formed by Nucleic Acid Binding Proteins: Using HP1 as a Model System. Curr Protoc *1*, e109.

Schaefer, A.M., Hadwiger, G.D., and Nonet, M.L. (2000). rpm-1, a conserved neuronal gene that regulates targeting and synaptogenesis in C. elegans. Neuron *26*, 345-356.

Schlutermann, D., Berleth, N., Deitersen, J., Wallot-Hieke, N., Friesen, O., Wu, W., Stuhldreier, F., Sun, Y., Berning, L., Friedrich, A.*, et al.* (2021). FIP200 controls the TBK1 activation threshold at SQSTM1/p62-positive condensates. Sci Rep *11*, 13863.

1179 Shin, J.E., Cho, Y., Beirowski, B., Milbrandt, J., Cavalli, V., and DiAntonio, A. (2012). Dual
1180 leucine zipper kinase is required for retrograde injury signaling and axonal regeneration.
1181 Neuron *74*, 1015-1022.
1182 Tanoue, T., Adachi, M., Moriguchi, T., and Nishida, E. (2000). A conserved docking motif in
1183 MAP kinases common to substrates, activators and regulators. Nat Cell Biol *2*, 110-116.
1184 Tanoue, T., Maeda, R., Adachi, M., and Nishida, E. (2001). Identification of a docking groove
1185 on ERK and p38 MAP kinases that regulates the specificity of docking interactions. EMBO J
1186 *20*, 466-479.
1187 Taylor, N.O., Wei, M.T., Stone, H.A., and Brangwynne, C.P. (2019). Quantifying Dynamics in
1188 Phase-Separated Condensates Using Fluorescence Recovery after Photobleaching.
1189 Biophys J *117*, 1285-1300.
1190 Tian, T., and Song, J. (2012). Mathematical modelling of the MAP kinase pathway using
1191 proteomic datasets. PLoS One *7*, e42230.
1192 Vizcaino, J.A., Deutsch, E.W., Wang, R., Csordas, A., Reisinger, F., Rios, D., Dianes, J.A.,
1193 Sun, Z., Farrah, T., Bandeira, N.*, et al.* (2014). ProteomeXchange provides globally
1194 coordinated proteomics data submission and dissemination. Nat Biotechnol *32*, 223-226.
1195 Widmann, C., Gibson, S., Jarpe, M.B., and Johnson, G.L. (1999). Mitogen-activated protein
1196 kinase: conservation of a three-kinase module from yeast to human. Physiol Rev *79*, 143-
1197 180.
1198 Wright, P.E., and Dyson, H.J. (2015). Intrinsically disordered proteins in cellular signalling
1199 and regulation. Nat Rev Mol Cell Biol *16*, 18-29.
1200 Yan, D., Wu, Z., Chisholm, A.D., and Jin, Y. (2009). The DLK-1 kinase promotes mRNA
1201 stability and local translation in C. elegans synapses and axon regeneration. Cell *138*, 1005-
1202 1018.
1203 Zarubin, T., and Han, J. (2005). Activation and signaling of the p38 MAP kinase pathway.
1204 Cell Res *15*, 11-18.
1205 Zhang, J.Z., Lu, T.W., Stolerman, L.M., Tenner, B., Yang, J.R., Zhang, J.F., Falcke, M.,
1206 Rangamani, P., Taylor, S.S., Mehta, S.*, et al.* (2020). Phase Separation of a PKA Regulatory
1207 Subunit Controls cAMP Compartmentation and Oncogenic Signaling. Cell *182*, 1531-1544
1208 e1515.
1209 Zhang, Y.Y., Mei, Z.Q., Wu, J.W., and Wang, Z.X. (2008). Enzymatic activity and substrate
1210 specificity of mitogen-activated protein kinase p38alpha in different phosphorylation states. J
1211 Biol Chem *283*, 26591-26601.
1212 Zhu, T., Xie, J., He, H., Li, H., Tang, X., Wang, S., Li, Z., Tian, Y., Li, L., Zhu, J.*, et al.*
1213 (2023). Phase separation underlies signaling activation of oncogenic NTRK fusions. Proc
1214 Natl Acad Sci U S A *120*, e2219589120.
1215
1216
1217
1218
1219